RSC Advances

PAPER

View Article Online
View Journal | View Issue

Cite this: *RSC Adv.*, 2026, **16**, 10451

Efficient removal of the ciprofloxacin drug using an electrospun Co/Al-layered double hydroxide-embedded chitosan/polyvinylidene fluoride nanofiber membrane

Fahad T. Alotaibi[a] and Ashraf A. El-Bindary *[bc]

The contamination of water by antibiotics due to the persistence and bioaccumulation of pharmaceutical compounds such as ciprofloxacin (CIP) is an environmental issue of great concern. This study focused on developing multifunctional nanofiber membranes by incorporating an Al/Co-layered double hydroxide (Co/Al-LDH) into a chitosan/polyvinylidene fluoride (CS/PVDF) matrix *via* the electrospinning technique for the efficient removal of CIP from water. The hybrid membrane synergized the high anion exchange and redox properties of Co/Al-LDH, the functionality brought about by the amino and hydroxyl groups in chitosan, and the stability provided by polyvinylidene fluoride. This led to the development of Co/Al-LDH–CS/PVDF with many active sites for adsorption by means of hydrogen bonding, electrostatic attraction, metal-ligand coordination, and fluorine-related interactions. Its full characterization *via* FT-IR, BET, XRD, SEM-EDX, XPS and 2D correlation FT-IR analyses validated the successful integration of Co/Al-LDH into the polymeric nanofibers and elucidated the adsorption mechanisms at the molecular level. Batch studies revealed a very high maximum adsorption capacity of 352.6 mg g^{-1} with rapid equilibrium at 40 min, pH-sensitive performance with the optimum pH of 6 and the adsorption being endothermic and spontaneous in nature. The isotherms and kinetic studies revealed that the adsorption process was predominantly monolayer chemisorption with a secondary contribution from multilayer interactions. Furthermore, response surface methodology (RSM) was actively employed for optimizing the operational parameters for practical applications. These membranes also have stability and the potential for reusability, as well as multifunctional biomedical applications. This shows that the Co/Al-LDH–CS/PVDF nanofiber membrane can be used effectively as a large-scale and sustainable adsorbent for treating pharmaceutical wastewater.

Received 14th November 2025
Accepted 29th January 2026

DOI: 10.1039/d5ra08795c

rsc.li/rsc-advances

1. Introduction

The pollution caused by antibiotics has emerged as a major environmental concern in the 21st century mainly because of the overuse and incorrect disposal of pharmaceutical substances in the healthcare, veterinary, and agricultural practices.[1] Ciprofloxacin (CIP) is a widely used fluoroquinolone antibiotic that has been detected in water bodies at concentrations ranging from nanograms to mg L^{-1}. Its environmental persistence, low biodegradability, and high potential for bioaccumulation raise significant concerns due to its possible adverse effects on aquatic ecosystems, the promotion of antimicrobial resistance, and eventual serious threat to human health.[2] As a result, finding efficient and long-lasting ways to remove the drug residues from wastewater has become an urgent issue worldwide. Common treatment methods such as flocculation, coagulation, chlorination, and biological breakdown usually do not completely eliminate antibiotics such as CIP because of their complicated molecular structures and resistance to decomposition.[3] On the other hand, advanced oxidation processes and membrane filtration technologies have shown good performance results, but they are limited by their high operational costs and energy requirements and the possibility of secondary pollution. Thus, adsorption-based methods are gaining increasing attention due to their simplicity, efficiency, low cost, and potential for regeneration. However, adsorption is highly dependent on the design and development of suitable adsorbents with high capacity, selectivity, and reusability.[4]

Layered double hydroxides (LDHs) have been widely accepted for their efficiency in environmental remediation due to their unique structural features, tunable composition, high

[a]*Department of Anatomy and Physiology, College of Medicine, Imam Mohammad Ibn Saud Islamic University (IMSIU), Riyadh 13317, Saudi Arabia*
[b]*Health Sciences Research Center (HSRC), Deanship of Scientific Research, Imam Mohammad Ibn Saud Islamic University (IMSIU), Riyadh 13317, Saudi Arabia*
[c]*Chemistry Department, Faculty of Science, Damietta University, Damietta 34517, Egypt. E-mail: abindary@du.edu.eg*

anion exchange capacity, and surface functionalities. Co/Al-LDH is particularly interesting as a potential candidate for environmental applications due to its combination of the stability of aluminum and the redox-active properties of cobalt, which allows different interaction mechanisms with pollutants.[5] However, unmodified LDHs often face problems such as clumping, small surface area, and lack of mechanical strength, which hinder their effective application in real-world wastewater treatment systems. To address these issues, researchers have proposed the embedding of LDHs into polymeric nanofiber membranes as a promising method to enhance their structural stability, surface accessibility, and adsorption performance.[6]

Electrospinning is a highly effective process for producing nanofiber membranes with interconnected porous networks, large surface-to-volume ratios, and tunable physicochemical properties.[7] The use of layered double hydroxides as functional fillers in electrospun polymer matrices leads to hybrid systems with improved properties, where the polymer contributes mechanical flexibility and easy processing, while the LDH provides active sites for adsorption. Polyvinylidene fluoride, known for its hydrophobic nature and chemical stability as well as its excellent fiber-forming ability, is combined with chitosan, a natural biopolymer containing abundant amino and hydroxyl groups, to form an ideal matrix supporting Co/Al-LDH nanoparticles. It is expected that the resultant Co/Al-LDH–CS/PVDF nanofiber membrane will exhibit the advantages of the adsorption properties of LDHs together with the biocompatibility and functional groups from CS and reinforced by the structural strength from PVDF.

The Co/Al-LDH-based composites can adsorb ciprofloxacin from water through diverse mechanisms like electrostatic attraction, hydrogen bonding, coordination between the metal and ligand, and π–π interactions.[8] The presence of amino and hydroxyl groups in chitosan, together with the layered structure of LDH and fluorine-rich polyvinylidene fluoride, creates different types of active sites. These active sites can readily interact with the carboxyl, piperazinyl, and quinolone functional groups of ciprofloxacin (CIP). These diverse interaction capabilities not only improve the adsorption efficiency but also increase the selectivity towards CIP over other organic contaminants. In addition, embedding LDH in nanofibers minimizes the leaching risks for nanoparticles, which is good for environmental safety as well as operational stability in water treatment processes.[9]

Recent studies have emphasized the importance of using advanced characterization techniques to fully understand the structure–property relationships in hybrid adsorbents. Several key techniques, including FT-IR, XRD, SEM, XPS, EDX, and BET surface area analysis, are critical in providing information about the functional groups, crystalline structure, surface morphology, elemental composition, and porosity of the prepared nanofiber membranes. Additionally, the study of adsorption isotherms, kinetics, and thermodynamic models plays an important role in understanding the interaction mechanisms between CIP and the adsorbent to establish whether the adsorption process is characterized by physisorption, chemisorption or both. These comprehensive studies are necessary for material design optimization and predictive capability regarding the actual field performance of these materials for wastewater treatment applications.

Apart from the processes related to the design and characterization of materials, different optimization methodologies, especially response surface methodology and Box–Behnken design, have been widely used for improving the performance of adsorbent systems. These statistical methods allow a systematic study of the effects of several limits such as pH, initial concentration, contact time, and amount of adsorbent. Accordingly, it is possible to find the best operating conditions as well as develop predictive models. Also, by using these methodologies in Co/Al-LDH–CS/PVDF systems, one can not only get a quantitative assessment of their adsorption potential but also derive practical information that helps in scaling up for their industrial use.

The development of Co/Al-LDH–CS/PVDF multifunctional nanofiber membranes goes beyond environmental remediation. The biocompatibility, structural tunability, and high drug loading efficiency of these membranes indicate their great potential for biomedical applications such as controlled drug delivery systems, antimicrobial coatings, and wound healing solutions. The dual functionalities of these materials further emphasize their broad relevance by bridging both the environmental and biomedical fields. More specifically with ciprofloxacin, an environmental pollutant as well as a clinically important antibiotic, merging these two perspectives creates an innovative platform for designing advanced functional materials with interdisciplinary benefits.

This study presents the preparation of a new multifunctional electrospun nanofiber membrane with Co/Al-LDH embedded in a CS/PVDF matrix for the removal of CIP from water under actual conditions. Its novelty lies in the synergistic effect of its three components: (i) high anion exchange capacity and redox-active properties of Co/Al-LDH, (ii) biocompatibility and functional groups provided by chitosan, and (iii) stability due to fluorine-rich nature of PVDF. This integration offers plenty of different active sites that favor multi-faceted adsorption mechanisms such as hydrogen bonding, electrostatic attraction, metal–ligand coordination and fluorine interactions. Herein, extensive spectroscopy and microscopy analyses including FT-IR, XRD, BET, SEM-EDX, and XPS with 2D correlation FT-IR techniques (synchronous and asynchronous) were used to improve the understanding in this field regarding the molecular-scale adsorption mechanism, which is rarely discussed in CIP removal studies. The application of response surface methodology (RSM) for process optimization further indicates the practical applications of the composite membrane by connecting fundamental insights on mechanisms to efficient strategies for water treatment.

2. Experimental

2.1. Resources and instruments

The details of the substances and equipment used are described in detail in Tables S1 and S2, respectively.

2.2. Adsorbent synthesis

2.2.1. Co/Al-LDH synthesis. Co/Al-layered double hydroxide (Co/Al-LDH) was prepared *via* the coprecipitation method. In the first step, solution A was prepared by dissolving 11.04 mmol (2.62 g) of cobalt chloride hexahydrate ($CoCl_2 \cdot 6H_2O$) and 4.9 mmol (0.655 g) of aluminum chloride ($AlCl_3$) in 50 mL of deionized water.[10] Simultaneously, 5.0 mmol (0.53 g) sodium carbonate (Na_2CO_3) and 26.35 mmol (1.054 g) sodium hydroxide (NaOH) were dissolved in 50 mL of double-distilled water to afford solution B. Solution B was slowly added to solution A during the experiment, with pH adjustments to maintain it between 9 and 10. The resulting mixture was stirred continuously at room temperature under a nitrogen atmosphere for one day. Co/Al-LDH powder was obtained by drying the precipitate in a furnace set at 60 °C after the reaction. The particles were then subjected to several cycles of centrifugation with ethanol followed by deionized water to remove excess ions (Fig. 1).

2.2.2. Co/Al-LDH–CS/PVDF nanofiber membrane synthesis. The nanofiber membrane structure was created by the electrospinning method using a polymer blend of polyvinylidene fluoride (PVDF) and chitosan (CS) at a weight ratio of 80 : 20.[11] The polymer solution at a concentration of 15% w/v was formulated by dissolving the constituents in a solvent comprised of 90% acetic acid and containing 5% w/w Co/Al-LDH. This was maintained in a glass syringe equipped with a blunt-tip 20-gauge needle.[12] The flow of the polymer solution was controlled at 1 mL h^{-1} using a syringe pump. A voltage between 27 and 28.5 kV was applied, with a needle-to-plate distance of 15 cm from the grounded collecting plate (Fig. 2). Electrospinning was performed under carefully controlled ambient conditions to achieve reproducible fiber production. The temperature was maintained at 25 °C ± 1 °C and relative humidity between 45% and 55% for all experiments. These environmental conditions ensured stable jet behavior and the production of bead-free nanofiber membranes.

2.3. Batch studies for the removal of CIP using Co/Al-LDH–CS/PVDF nanofiber membrane

To analyze the adsorption models, 0.02 g of Co/Al-LDH–CS/PVDF nanofiber membrane was mixed with a 25 mL solution of ciprofloxacin (CIP) at concentrations varying from 35 to 430 mg L^{-1}. The pH of the medium was precisely adjusted to 8 using dilute sodium hydroxide. This mixture was then placed in a water bath oscillator set at 200 rpm and maintained at an even temperature of 25 °C. Samples were taken systematically at certain times between 5 and 100 min to explore the adsorption characteristics.[13] The sample solutions were centrifuged, and the CIP concentrations were determined using a UV spectrophotometer set at 272 nm. The adsorption capacity (q_e in mg g^{-1}) and the removal efficiency of CIP (R in %) were calculated using eqn (1) and (2), respectively.

$$\% \ R = \frac{(C_0 - C_t)}{C_0} \times 100 \quad (1)$$

$$q_e = \frac{(C_0 - C_e) \times V}{M} \quad (2)$$

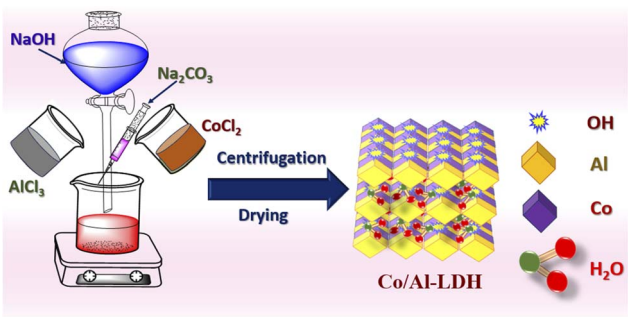

Fig. 1 Schematic of the synthesis of the Co/Al-LDH adsorbent.

2.4. Biological experiments

The cell lines used in this study were obtained from a well-established cell bank. More specifically, the MCF-7 cell line, which stands for human breast adenocarcinoma, and HepG-2, representing human hepatocellular carcinoma, were both supplied by the American Type Culture Collection (ATCC located at Manassas Virginia USA). These particular lines were maintained under the conditions recommended by their provider.

2.5. Investigational design

The Box–Behnken design (BBD) is a popular experimental design method used to study responses in detail. This involves creating a valid model that reflects the observed data, which will help in determining the interactions between independent variables, including amount of adsorbent, pH, and contact time, necessary for the efficient removal of CIP.[14,15] A significant part of this plan is performing adsorption tests using the BBD design, with help from the Design-Expert Version 13 software (Stat-Ease). The data shows the levels of factors considered and the codes given to each level. Also, applying second-degree polynomial modeling to examine the connections between independent variables and a dependent outcome is an essential part of this strategy, as shown in eqn (3):

$$Y = \beta_o + \sum \beta_i X_i + \sum \beta_{ii} X_i^2 + \sum\sum \beta_{ij} X_i X_j, \quad (3)$$

where the X_i and X_j variables represent the elements being analyzed, whereas Y denotes the outcome being assessed, which in this instance is characterized by CIP. A total of 17 well-structured trials were conducted for the documented elimination process. Each study began with the assessment of CIP removal by mixing 25 mL of CIP solution with a precisely measured quantity of Co/Al-LDH–CS/PVDF nanofiber membrane, as detailed in Table S3.

Response surface methodology is regarded as a powerful optimization technique for identifying the optimal interactions between several factors that lead to the maximization or minimization of certain responses. Box–Behnken design is one of

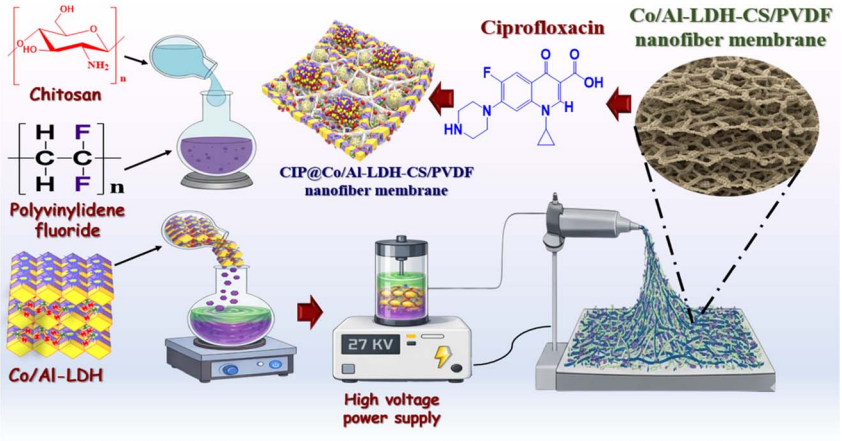

Fig. 2 Schematic of the preparation of the Co/Al-LDH–CS/PVDF nanofiber membrane.

the most widely utilized experimental designs in RSM.[16] This design extracts first- and second-order values from three-level incomplete factorial designs through mathematical models. The application of this design appears in the adsorption capacity optimization study considering time, dosage, and pH. Herein, three stages of study of zero, positive and negative were implemented. In general terms, RSM provides scientists with the necessary tools to investigate and find optimal solutions for their problems, as shown in Table 1.

3. Results and discussion

3.1. Characterization of Co/Al-LDH–CS/PVDF

3.1.1. X-ray diffraction patterns (XRD). The X-ray diffraction results for Co/Al-LDH, CS/PVDF nanofiber membrane, and Co/Al-LDH–CS/PVDF composite nanofiber membrane show very clearly the structural properties and the successful loading of the layered double hydroxide into the polymer matrix.[17–19] The pure Co/Al-LDH shows clear and sharp diffraction peaks, especially at about $2\theta = 11°$ and 23°. These peaks correspond to the (003) and (006) planes of hydrotalcite-like LDHs, respectively, and confirm that Co/Al-LDH has high crystallinity with a well-ordered layered structure. On the other hand, the CS/PVDF nanofiber membrane presents broader diffraction peaks, including those at around $2\theta = 20°$ and 26°, which are related to the β and α crystalline phases of PVDF, respectively, as well as the amorphous features of chitosan. This shows the partially crystalline and partially non-crystalline character of the electrospun polymer. After adding Co/Al-LDH into the CS/PVDF mixture, the new composite membrane displayed a mix of these clear traits. The typical peaks of LDH are still present but more blurred and less intense, while the peaks for the polymer slightly change also. The broadening of this peak and its decrease in intensity suggest that the long-range order of the LDH is partially disrupted due to its confinement within the polymer fibers, accompanied by strong interfacial interactions between the LDH particles and CS/PVDF chains. These structural changes indicate the effective dispersion of LDH within the nanofiber network, thereby enhancing the stability and compatibility of the composite membrane which are both required for the removal of CIP (Fig. 3(a)).

Table 1 Adsorption capacity of CIP studied utilizing BBD and RSM design

	Actual variables			q_e (mg g^{-1})		
Run	Dose (g)	Time (min)	pH	Experimental	Predicted	Residue
1	0.26	52.5	7	238.11	238.11	0.0000
2	0.02	52.5	2	193.46	195.62	−2.15
3	0.26	52.5	7	238.11	238.11	0.0000
4	0.5	52.5	12	162.92	160.76	2.15
5	0.26	5	12	3.73	−14.50	18.23
6	0.5	100	7	220.50	201.99	18.51
7	0.02	5	7	5.60	24.11	−18.51
8	0.02	100	7	352.80	332.41	20.39
9	0.26	52.5	7	238.11	238.11	0.0000
10	0.26	52.5	7	238.11	238.11	0.0000
11	0.5	52.5	2	147.40	147.67	−0.2730
12	0.5	5	7	3.50	23.89	−20.39
13	0.26	100	2	180.00	198.23	−18.23
14	0.02	52.5	12	243.73	243.46	0.2730
15	0.26	100	12	235.20	255.86	−20.66
16	0.26	52.5	7	238.11	238.11	0.0000
17	0.26	5	2	2.85	−17.81	20.66

3.1.2. N_2 adsorption/desorption isotherms. The nitrogen adsorption–desorption isotherm and pore structure evaluation analysis results give essential information about the textural properties of the materials before and after the adsorption of CIP. The two samples display a type IV isotherm with an H3-type hysteresis loop, as illustrated in Fig. 3(b), which indicates mesoporous characteristics with slit-like pores formed by the arrangement of layered structures with nanofiber networks.[19,20] This reflection supports the presence of a strong mesoporous structure in the nanofiber membrane, which increases its drug adsorption capability and helps transport the drug. The pore radius distribution, as shown in Fig. 3(c), reveals that the initial Co/Al-LDH–CS/PVDF membrane had an average pore radius of 2.36 nm. After CIP adsorption, this average pore radius decreased to 1.98 nm, indicating that the drug molecules

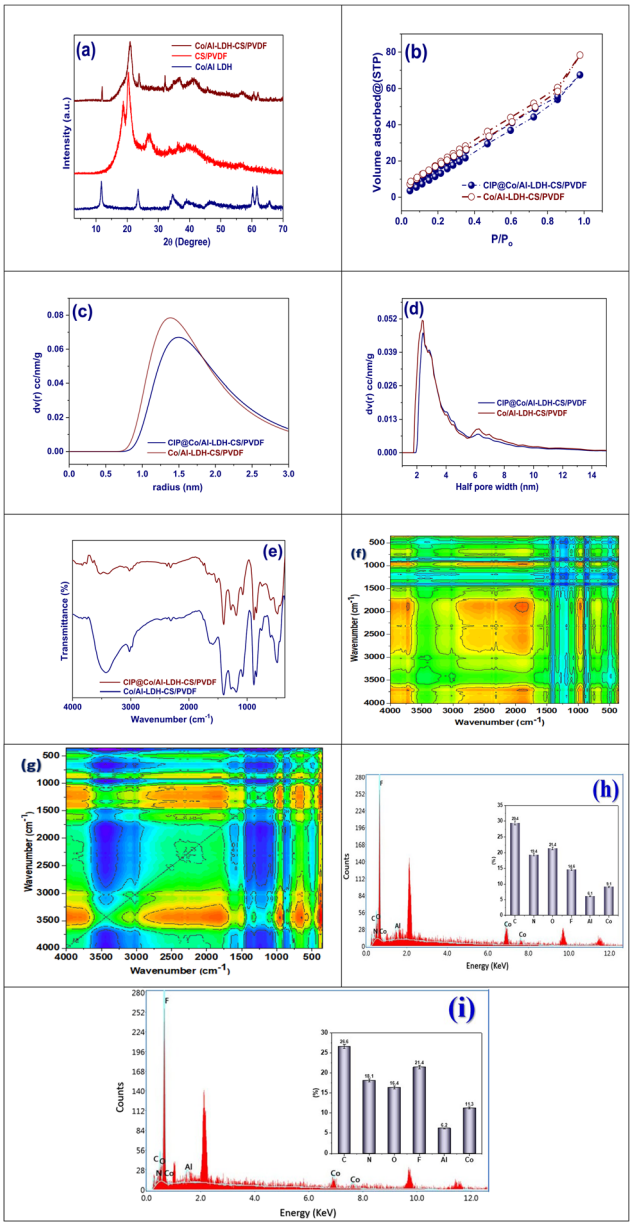

Fig. 3 (a) XRD patterns of the CS/PVDF membrane, Co/Al-LDH, and the Co/Al-LDH–CS/PVDF nanofiber membrane. (b) N_2 adsorption/desorption isotherms of Co/Al-LDH–CS/PVDF and CIP@Co/Al-LDH–CS/PVDF. (c) Pore radius, (d) pore size distribution and (e) FT-IR spectra of Co/Al-LDH–CS/PVDF and CIP@Co/Al-LDH–CS/PVDF. (f) Synchronous map and (g) asynchronous map of the Co/Al-LDH–CS/PVDF and CIP@Co/Al-LDH–CS/PVDF nanofiber membrane. (h) EDX analysis of the Co/Al-LDH–CS/PVDF membrane, and (i) EDX analysis of the CIP@Co/Al-LDH–CS/PVDF membrane.

partially blocked its pores. The pore size distribution shown in Fig. 3(d) reveals a slight narrowing of the mesoporous range after adsorption, indicating reduced access to the pore channels within the Co/Al-LDH–CS/PVDF nanofiber membrane due to CIP retention. The Co/Al-LDH–CS/PVDF nanofiber membrane has a surface area of 98.76 $m^2\ g^{-1}$ and total pore volume of 0.14 $cm^3\ g^{-1}$, which decrease after CIP adsorption to 92.6 $m^2\ g^{-1}$ and 0.11 $cm^3\ g^{-1}$, respectively. This observed reduction in surface area, pore size, and pore volume serves as clear evidence for the actual uptake of CIP into the porous structure of the nanofiber membrane. It confirms that the adsorption process is mainly controlled by surface interactions and pore-filling mechanisms. These results highlight the mesoporous characteristics of the composite membrane and its ability to adsorb and hold ciprofloxacin firmly.

3.1.3. FT-IR spectroscopy. The FT-IR spectra presented in Fig. 3(e) provide strong proof for the adsorption of CIP on the Co/Al-LDH–CS/PVDF nanofiber membrane, as shown by the significant changes in its characteristic vibrational bands. In the spectrum of the original Co/Al-LDH–CS/PVDF membrane, the broad absorption band at about 3400 cm^{-1} represents the O–H and N–H stretching vibrations from the hydroxyl groups in chitosan and interlayer water of the LDH. The peaks at around 2920 and 2850 cm^{-1} are due to C–H stretching from the $-CH_2$ groups in both PVDF and chitosan. The band close to 1660 cm^{-1} is related to amide I, which indicates C=O stretching in chitosan, which is overlapped by the H–O–H bending vibrations of water.[21,22] Also, the large peak at about 1415 cm^{-1} is related to the vibrations of interlayer carbonates from the LDH structure. The strong absorption in the range of 1180–1070 cm^{-1} is related to the C–F stretching of PVDF and C–O–C bonding in chitosan. The bands below 800 cm^{-1} are associated with the Al–O and Co–O lattice vibrations.[23,24] After the adsorption of CIP, new and intense bands appear, where the band at around 1720 cm^{-1} confirms the C=O stretching of carboxyl groups from CIP, and the bands with increased intensity at 1620–1640 cm^{-1} corresponds to the quinolone C=C skeletal stretching and N–H bending from the piperazine part of CIP, which overlaps with the amide bands of chitosan. The broadening in the hydroxyl region observed at 3400 cm^{-1} suggests very strong hydrogen bonding between the functional groups of CIP and matrix rich in hydroxyls created by LDH and chitosan. Also, the changes in the carbonate band at about 1415 cm^{-1} show electrostatic interactions between the carboxylate groups of CIP and the positively charged layers of LDH. The changes in the fingerprint region (1100–1000 cm^{-1}) show that there is an overlap between the C–F stretching of PVDF and the fluorinated quinolone group of CIP. The appearance of new small bands below 800 cm^{-1} provide more proof for interactions between vibrations from the aromatic ring in CIP with metal–O bonds.[25] In summary, these spectral variations suggest that CIP immobilization occurs *via* several pathways including hydrogen bonding, electrostatic interaction, coordination with metal centers, and fluorine-related interactions. This highlights the potential of Co/Al-LDH–CS/PVDF for effective adsorption.

The 2D correlation FT-IR spectra describe the adsorption mechanism of CIP on the Co/Al-LDH–CS/PVDF nanofiber membrane by reflecting both the concurrent and consecutive changes in functional groups. In the synchronous map presented in Fig. 3(f), distinct auto peaks can be observed at about 3400, 1650–1600, 1400, and 1100–1000 cm^{-1}. These peaks are attributed to O–H/N–H stretching, amide/quinolone C=O and N–H vibrations, interlayer carbonate groups of the LDH, and functionalities corresponding to PVDF (C–F) and chitosan (C–O–C), which reveal maximum intensity variations after

adsorption. The positive cross-peaks between measurements at 3400 and 1650 cm^{-1} denote an interaction between the hydroxyl groups and amide/aromatic vibrations of CIP; this implies that besides electrostatic interactions, hydrogen bonding is also involved. Moreover, the correlations in the 1650 and 1400 cm^{-1} regions indicate the coupling of the C=O/N–H groups with carbonate species, which supports electrostatic binding. The interaction of the aromatic/quinolone moieties of CIP with the polymer matrix (C–F and C–O–C) is suggested by correlations between 1650 and 1100–1000 cm^{-1}, which correspond to π–π stacking as well as fluorine-related effects. On the other hand, the negative cross-peaks between hydroxyl or carbonate bands and polymer region confirm that CIP coverage over the surface reduces the PVDF vibration contribution due to competition among functional groups during adsorption.

The asynchronous spectrum presented in Fig. 3(g) provides more information about the order of events taking place in the system. The presence of asynchronous cross-peaks in the range of 3400 to 1650 cm^{-1} indicates that the hydroxyl groups from chitosan and LDH interact first, before the amide and aromatic groups of CIP join in. This shows that hydrogen bonding is the main driving force behind these initial interactions. After this, the asynchronous relationships seen between 1650–1600 and 1400 cm^{-1} suggest that when the amide and carboxyl groups of CIP get involved, changes occur in the structure of the LDH carbonate, which corresponds with electrostatic exchange mechanisms.[26,27] The asynchronous correlations that were mentioned in the previous paragraph about 1650 and 1100–1000 cm^{-1} suggest more that interactions with the functionalities of the polymer, specifically the PVDF (C–F) and CS (C–O–C) groups, take place at a later stage to stabilize the immobilized drug molecules. Negative asynchronous signals also support this because they imply out-of-phase or competitive interaction between the LDH hydroxyl/carbonate sites and PVDF functionalities. This means that the polymer groups only come into play after the primary adsorption sites are filled.

The results of both the synchronous and asynchronous analyses converge in establishing that the mechanism governing the adsorption of CIP is multifaceted. The process begins with an initiation step involving hydrogen bonding through hydroxyl groups. This is followed by electrostatic interactions with the carbonate groups and metal centers, which contribute to the enhanced immobilization of the drug. Further stabilization comes from the polymeric functionalities. This detailed analysis corroborates the synergistic role played by LDH, chitosan, and PVDF in achieving efficient removal of CIP through complex multi-site interactions.

3.1.4. EDX analysis. Fig. 3(h) shows the energy dispersive X-ray (EDX) spectrum and the elemental composition table of the Co/Al-LDH–CS/PVDF nanofiber membrane which together confirm its formation. This provides quantitative details about its multi-component structure.[28] The spectrum shows strong peaks for fluorine (14.6%), mainly coming from the PVDF backbone, underscoring the importance of the polymer matrix in the composite material. The contributions of oxygen (21.4%) and carbon (29.4%), which come from both the chitosan chains and the hydroxyl/carbonate groups attached to the LDH, are important for this analysis. Nitrogen (19.4%) is associated with the amino groups present in chitosan, further confirming the addition of the biopolymer.[29] The presence of aluminum (6.1%) and cobalt (9.1%) confirms that the LDH was successfully embedded in the nanofiber structure. The relative abundance of cobalt indicates its important role in charge balancing and providing active sites for adsorption. Even though the EDX mapping is not shown here, it indicates a consistent distribution of these elements, which reflects a uniform dispersion of LDH particles throughout the CS/PVDF nanofiber matrix. Thus, in summary, the EDX analysis validates the structural composition of the composite membrane as being primarily made up of PVDF (rich in fluorine), supported by chitosan functionalities (carbon, oxygen, and nitrogen) and well-integrated Co/Al-LDH active phases, which together enhance the structural integrity while simultaneously providing numerous active sites for the adsorption of CIP.

The EDX spectrum and elemental composition table in Fig. 3(i) clearly show the adsorption of CIP onto the Co/Al-LDH–CS/PVDF nanofiber membrane. This is indicated by significant shifts in the elemental percentages from that of the unmodified material. After adsorption, the fluorine content increases substantially from 14.6% to 21.4%, which can be attributed to the incorporation of the fluorinated quinolone structure of CIP and hence confirms efficient drug immobilization. The content of cobalt (Co) and aluminum (Al) was measured to be 11.3% and 6.2%, respectively, indicating that the CIP molecules partially block access to the active metal sites on the LDH surface given that a lower EDX signal is observed for these metals. In addition, the nitrogen content decreases from 19.4% to 18.1%; this further proves bonding between the amine and piperazinyl groups of CIP with the chitosan–LDH matrix, implying the occurrence of electrostatic interactions and hydrogen bonding. The changes in composition observed here, particularly the large increase in fluorine and decrease in metal signals, confirm that CIP was successfully anchored within the nanofiber membrane by several different types of interactions including those related to fluorine, hydrogen bonding and coordination with the active centers of LDH.

3.1.5. SEM. The morphology and elemental distribution of the Co/Al-LDH–CS/PVDF nanofiber membrane are described in several figures, where Fig. 4(a) shows a grayscale 3D AFM map revealing a fibrous morphology with sharp ridges and interlinked pores; Fig. 4(b) is a thermal color scale AFM image that shows the difference in surface irregularity at nano heights; Fig. 4(c) presents green-tone AFM images, emphasizing the uniform orientation of nanofibers in a porous framework; Fig. 4(d) contains SEM micrographs taken at different magnifications, proving the presence of smooth and bead-free nanofibers with average diameters ranging from around 30 to about 150 nm, which indicates the reproducible electrospun morphology; Fig. 4(e) provides the SEM-EDX elemental mapping for the composite material, where elements such as C, N, O, F, Al, and Co are evenly distributed, confirming the proper incorporation of Co/Al-LDH–CS/PVDF matrix. The strong signal for fluorine (from PVDF) and substantial amounts of Al and Co also confirm the properties of the composite,

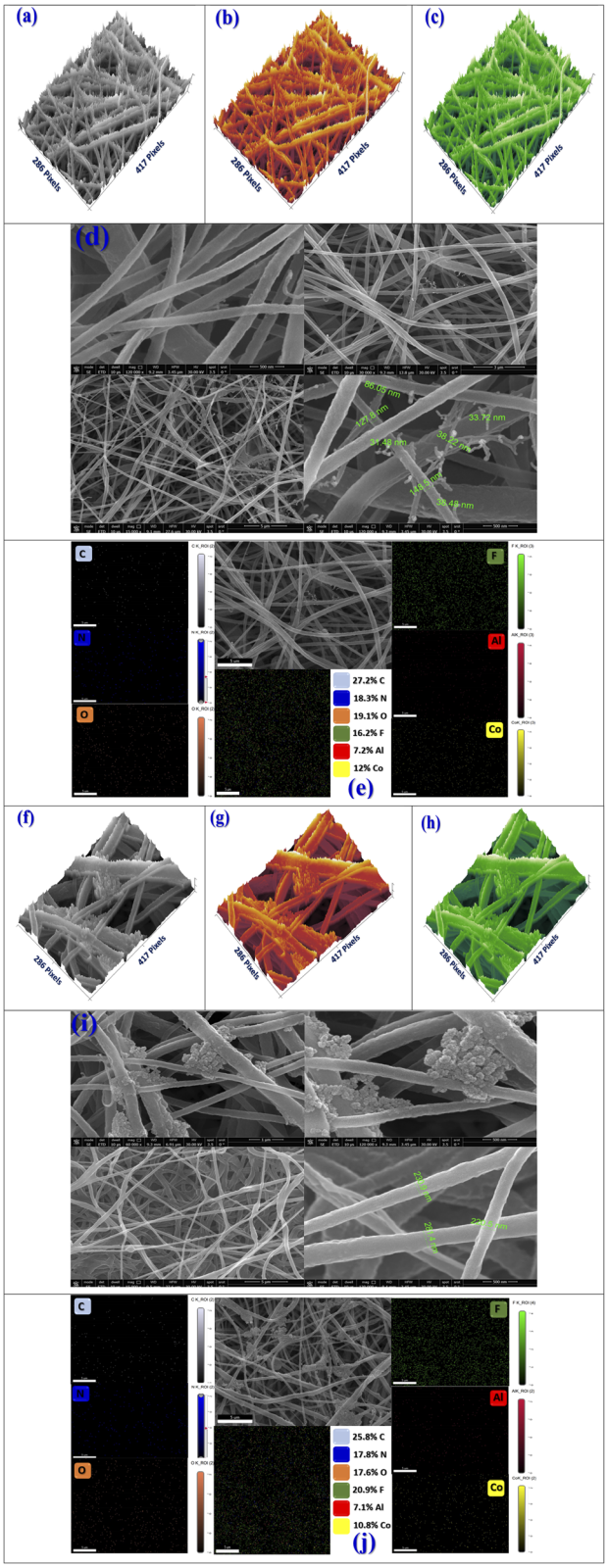

Fig. 4 (a) 3D grayscale map of Co/Al-LDH–CS/PVDF. (b) Scale of thermal color, (c) green tones, and (d) SEM images of Co/Al-LDH–CS/PVDF. (e) SEM elemental mapping of Co/Al-LDH–CS/PVDF. (f) 3D grayscale map of CIP@Co/Al-LDH–CS/PVDF. (g) Scale of thermal color, (h) green tones, and (i) SEM images of CIP@Co/Al-LDH–CS/PVDF. (j) SEM elemental mapping of CIP@Co/Al-LDH–CS/PVDF.

together with the presence of multifunctional active sites that favor the adsorption of ciprofloxacin.[30]

The surface morphology and elemental mapping of the CIP-loaded Co/Al-LDH–CS/PVDF nanofiber membrane are also presented in Fig. 4.[31] Fig. 4(f) presents a grayscale 3D AFM map, which shows the surface roughness and dense fiber structure after the adsorption of CIP. The thermal color scale AFM image in Fig. 4(g) indicates the height distribution and better textural properties of the membrane. A green-tone AFM image is shown in Fig. 4(h), revealing uniform fiber arrangements as well as surface changes due to CIP deposition. SEM micrographs at different magnifications are provided in Fig. 4(i), highlighting the presence of bead-free interconnected nanofibers with an increased surface.[31] Roughness and visible aggregates of CIP can be observed, with fiber diameters of about 220 to 280 nm. Finally, Fig. 4(j) shows the SEM-EDX mapping, which proves the existence of C, N, O, F, Al, and Co with an increased oxygen content, thus validating the successful immobilization of CIP molecules on the nanofiber structure. The even distribution of particles assures the actual incorporation of Co/Al-LDH into the CS/PVDF matrix and indicates a solid interaction between the functional groups of CIP and the surface of the adsorbent.[31]

3.1.6. XPS. The C 1s X-ray photoelectron spectra for the Co/Al-LDH–CS/PVDF nanofiber membrane before and after the adsorption of CIP show significant changes in the chemical environment of the carbon species. This indicates that adsorption has indeed taken place. In the unmodified Co/Al-LDH–CS/PVDF membrane, the C 1s spectrum reveals peaks at 284.81 eV (25.18%), which are associated with the C–C/C–H bonds from PVDF and chitosan; the peak at 286.35 eV (39.53%) corresponds to the C–O/C–N groups from chitosan and LDH hydroxyl linkages; at 288.91 eV (13.08%) corresponds with the C=O groups; and finally at 290.9 eV (22.21%), which is linked to the O–C=O functionalities and carbonate species. After CIP adsorption (CIP@Co/Al-LDH–CS/PVDF), major changes occur in the relative intensities of the peaks. The C–C/C–H peak has shifts to 284.65 eV (15.24%), which signifies surface coverage by aromatic carbons from CIP. On the other hand, more contribution comes from C–O/C–N, as the intensity of the peak at 286.12 eV (50.49%) increases sharply. This indicates strong bonding between the amine and hydroxyl groups of CIP with the functional groups in the nanofibers. The O–C=O peak shifts slightly from its position at 290.9 to 290.65 eV with a reduction in its intensity (34.27%); this indicates that the carboxyl groups of CIP are involved in binding through mechanisms such as hydrogen bonding and electrostatic attraction. These spectral changes clearly demonstrate that adsorption takes place *via* multiple devices involving electrostatic interactions, π–π stacking, and hydrogen bonding, with the observed redistributions in intensities and peak shifts serving as direct evidence for chemical interactions between the drug and Co/Al-LDH–CS/PVDF.[32,33]

The O 1s XPS spectra of the Co/Al-LDH–CS/PVDF nanofiber membrane before and after the adsorption of CIP show clear changes in the oxygen chemical environment. This highlights the strong interaction between the drug and the surface of the composite. In its initial state, the Co/Al-LDH–CS/PVDF

membrane shows two main peaks at 531.42 eV (82.01%), which are attributed to lattice oxygen species (M–O bonds from Al–O and Co–O within the LDH structure), and at 532.96 eV (17.99%) related to the surface hydroxyl groups as well as oxygen-containing functional groups contributed by chitosan and PVDF. A clear reallocation of oxygen species in the spectrum can be seen after CIP adsorption; specifically, the intensity of the lattice oxygen peak is reduced, while a peak emerges at 532.58 eV (72.91%) with a more pronounced intensity, revealing that the surface hydroxyl groups and some functionalities from chitosan are now engaged in hydrogen bonding and electrostatic interactions with the CIP molecules. Also, another new high-binding energy peak at 534.97 eV (27.09%) is observed; this peak is associated with the carboxyl (–COOH) and carbonyl (C=O) oxygen atoms of ciprofloxacin, which confirms that ciprofloxacin was successfully attached to the membrane surface. These changes in position and intensity indicate that the adsorption of ciprofloxacin mostly happens through interaction between its functional groups and the oxygenated hydroxyl-rich LDH–chitosan matrix *via* mechanisms such as hydrogen bonding, electrostatic attraction, and possible coordination with the Co/Al metal centers, thereby proving the effectiveness of the Co/Al-LDH–CS/PVDF nanofiber membrane as an adsorbent for the removal of pharmaceuticals.[34,35]

The N 1s XPS spectra of the Co/Al-LDH–CS/PVDF nanofiber membrane before and after CIP adsorption show the important role played by nitrogen in this adsorption device. In the pristine Co/Al-LDH–CS/PVDF membrane, the N 1s peak is located at 398.99 eV. This can be assigned to amine ($-NH_2$) and amide-type nitrogen functionalities from chitosan plus nitrogen from the LDH structure. This peak shows that these groups are present as active sites for interaction. However, after CIP adsorption, this peak shifts to a higher binding energy of 400.61 eV, which indicates a change in chemical environment near the N atoms; it is related to the secondary amine and piperazine nitrogen interactions with hydroxyl groups on chitosan and Co/Al-LDH surface, confirming hydrogen bond formation, electrostatic interaction, and possibly coordination with the metal centers. The increase in binding energy observed indicates that the N atoms of CIP are either protonated or participate in stronger polar interactions; this supports the fact that both chitosan and CIP nitrogen functionalities play important roles in the adsorption process. These spectral shifts, together with the analyses of the C 1s and O 1s regions, further confirm the important role played by nitrogen in stabilizing the binding of CIP on the nanofiber membrane through the synergistic interaction among LDH, chitosan, and PVDF for the removal of this pharmaceutical.[36,37]

X-ray photoelectron spectroscopy of aluminum in the Co/Al-LDH–CS/PVDF nanofiber membrane before and after CIP adsorption shows strong changes in the electronic state of aluminum. This confirms that aluminum takes part in the chemical reaction during adsorption. In the bare membrane, a clear Al 2p peak is seen at 75.73 eV, which is characteristic for the Al^{3+} species inside the LDH structure and indicates coordination between aluminum and hydroxyl groups (Al–OH). This result proves that the outline structure of the LDH was maintained. After CIP adsorption, the Al 2p peak shifted slightly to 75.63 eV, indicating a new chemical environment around the Al^{3+} ions due to their interaction with the drug molecules.[38] This negative shift indicates an electron density rearrangement, probably due to electrostatic attraction or coordination between the carboxylate and carbonyl groups of CIP and the positively charged Al^{3+} ions. Although the oxidation state of aluminum remains unchanged, this peak shift implies that the Al sites are actively involved in the binding process. This observation aligns with the interactions observed in the C 1s, O 1s, and N 1s spectra, providing additional evidence that CIP adsorption on the membrane surface is governed by a complex mechanism that involves multiple sites such as metal centers, hydroxyl groups, and drug-specific functional moieties (Fig. 5).

The Co 2p XPS spectra of the Co/Al-LDH–CS/PVDF nanofiber membrane prior to and after CIP adsorption provide important insights into the role of cobalt in the adsorption mechanism. The Co 2p spectrum of the unmodified Co/Al-LDH–CS/PVDF membrane shows well-resolved peaks attributed to Co^{2+} and Co^{3+} states, confirming that cobalt is indeed present in a mixed valence state within the layered double hydroxide structure. This property is essential for maintaining charge balance and providing active sites. After CIP was adsorbed, subtle shifts in binding energies and changes in peak intensities were observed in the Co 2p region, which reflect changes in the electronic environment around the cobalt species. These changes suggest that the adsorption sites are actively involved, probably by means of electrostatic interactions as well as coordination with the functional groups of CIP, especially its carboxylate oxygen and nitrogen atoms.[39] The changes seen in the Co 2p spectra after adsorption support the idea that CIP interacts not only with the surface hydroxyl groups and aluminum centers but also with the cobalt ions, thus contributing to an adsorption mechanism involving multiple sites. The overall analysis of the Co 2p spectra agrees with the findings from the C 1s, O 1s, N 1s, and Al 2p spectra. This means that both the aluminum and cobalt metal centers, together with the functional groups of the polymer matrix help ciprofloxacin to get immobilized onto the nanofiber membrane, as shown in Fig. 5.

The F 1s XPS analysis of the Co/Al-LDH–CS/PVDF nanofiber membrane, before and after CIP adsorption, shows clear changes that prove the drug was added and interacted with the composite structure. In the F 1s spectrum of the unmodified Co/Al-LDH–CS/PVDF membrane, the peak located at 687.5 eV is mostly due to the $-CF_2$ groups in the PVDF backbone. This indicates the stable presence of fluorine in the polymer matrix. On the other hand, after CIP adsorption, there is a clear shift in the F 1s peak to 688.42 eV and a large increase in its intensity; this increase in binding energy means more fluorine atoms are added from CIP, which has a fluorinated quinolone ring. The shift and increased peak intensity show changes in the environment of fluorine due to strong interactions between CIP and the nanofiber membrane. This observation can serve as evidence that apart from some inherent contribution from PVDF itself, any signal of fluorine in the composite loaded with CIP must come from the adsorbed drug. Additionally, the

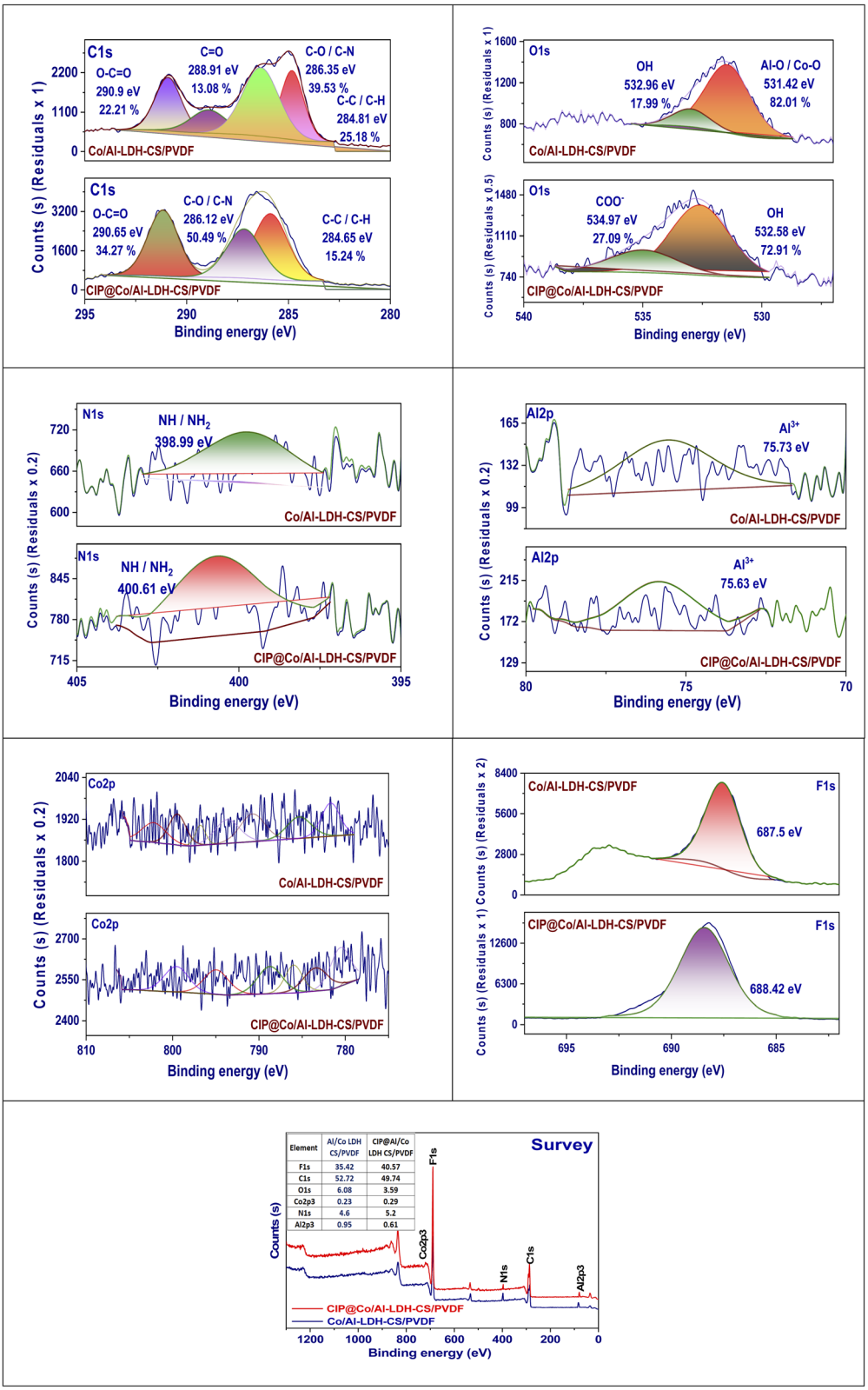

Fig. 5 XPS analysis of the Co/Al-LDH–CS/PVDF and CIP@Co/Al-LDH–CS/PVDF nanofiber membranes.

positive shift in binding energy indicates electronic interactions between the fluorinated groups of CIP and functional groups in the Co/Al-LDH–CS/PVDF matrix, strengthening the complex adsorption mechanism involving hydrogen bonding, electrostatic interaction, metal coordination, and that related to fluorine.

The wide-scan XPS survey spectra of the Co/Al-LDH–CS/PVDF nanofiber membrane before and after the adsorption of CIP show major compositional changes, confirming the effective removal and immobilization of the drug. In its original state, the membrane exhibits a significant elemental distribution with C 1s at 52.72% from PVDF and the chitosan framework and F 1s at 35.42% from the characteristic $-CF_2$ of PVDF.[40] Also, smaller fractions include O 1s at 6.08% for hydroxyl groups, N 1s at 4.6% due to chitosan, and very tiny amounts of Co $2p_3$ at 0.23% and Al $2p_3$ at 0.95%, which are related to the layered double hydroxide component. After the adsorption of CIP, the survey spectrum reveals large changes; the F 1s atomic percentage increases significantly from 35.42% to 40.57%, providing direct evidence that CIP molecules with a fluorinated quinolone ring were incorporated into the composite because they contain this ring. At the same time, the N 1s content increases from 4.6% to 5.2%, showing that nitrogen atoms from the piperazinyl group of CIPs are now present, while O 1s content drops from 6.08% to 3.59%. This suggests that the hydroxyl groups from chitosan and LDH actively participate in binding through hydrogen bonding and electrostatic interactions. The small changes in Co $2p_3$ (from 0.23% to 0.29%) and Al $2p_3$ (from 0.95% to 0.61%) further indicate interactions between CIP and the metal centers of the LDH. The C 1s fraction shows a small drop from 52.72% to 49.74%, indicating that it is partly covered on the surface by this drug (Fig. 5).

3.1.7. Point of zero charge. Fig. 6(a) presents the determination of point of zero charge (pH_{pzc}) for the Co/Al-LDH–CS/PVDF nanofiber membrane. In this figure, the change in pH ($\Delta pH = pH_{final} - pH_{initial}$) is plotted against various initial pH values. The curve obtained from this plot shows that at acidic pH, ΔpH takes a positive value, which indicates protonation of the surface functional groups and results in a net positive charge on the surface. As the initial pH increases, ΔpH decreases, and finally passes through zero at an inflection point located at pH 4.89; hence, this value can be taken as pH_{pzc}. This is also known as the point where there are no excess charges on the surface of the membrane; any movement to either side of this value will provide different surface charges (positive or negative). Above pH 4.89, the Co/Al-LDH–CS/PVDF nanofiber membrane surface becomes negatively charged due to deprotonation of the hydroxyl and amino groups in chitosan as well as hydroxyls on the LDH surface. In aqueous solutions above pH 4.89, CIP will mainly exist as cationic or zwitterionic species with protonated amine groups.[41] Therefore, the electrostatic attraction between the positively charged CIP particles and the negatively charged membrane surface is very strong. These charge-driven interactions significantly enhance the ability of the membrane to adsorb and selectively remove CIP. The relatively low pH_{pzc} of 4.89 is beneficial because it guarantees that under typical pH conditions in environmental and wastewater applications (5–8), the membrane surface will be negatively charged and highly efficient for the adsorption of ciprofloxacin *via* mechanisms involving electrostatic binding, H-bonding, and π–π interactions (Fig. 6(a)).

3.2. Batch experiments

3.2.1. Effect of pH. Fig. 6(b) shows how pH affects the CIP adsorption capacity of the Co/Al-LDH–CS/PVDF nanofiber membrane. There is a large difference in equilibrium uptake (q_e) when the solution pH changes. At very acidic pH 2, the adsorption capacity is low at 120 mg g^{-1} because at this pH the membrane surface is positively charged (since it is below its pH_{zpc} of 4.89). This leads to electrostatic repulsion between the protonated surface groups and the cationic form of CIP. As the pH increases towards neutrality, adsorption capability increases quickly and reaches the maximum value of 275 mg g^{-1} at pH 6.[42,43] The increase in adsorption is significant because the surface hydroxyl and amino groups are being deprotonated, thereby converting the membrane surface from a neutral to negatively charged state. This transformation increases the electrostatic attraction between both the cationic and zwitterionic forms of CIP with the membrane surface. Beyond pH 6, there is a minimal decrease in adsorption capacity (257 mg g^{-1} at pH 7 and 236 mg g^{-1} at pH 8); this can be attributed to the partial deprotonation of the CIP molecules under alkaline conditions, which reduces the electrostatic interactions. Overall, the findings indicate that optimal adsorption happens at pH 6, where the dynamics of surface charge relative to pH_{zpc} (4.89) create maximum conditions for such an attraction.

3.2.2. Effect of dose. The effect of adsorbent dose on adsorption capacity and removal efficiency for CIP using the Co/Al-LDH–CS/PVDF membrane is presented in Fig. 6(c). A clear inverse relationship exists between adsorption capacity (q_e, mg g^{-1}) and removal efficiency (%) as the dosage increases from 0.02 to 0.5 g/25 mL. At a very low dosage of 0.02 g/25 mL, the adsorption capacity is quite high at 343.75 mg g^{-1}, while the removal efficiency is only 68.75.[44] This is because the rapid saturation of imperfect adsorption sites occurs even when there is a significant concentration gradient. As the dose increases, the adsorption capacity per unit mass decreases significantly, with a value of 19.6 mg g^{-1} at 0.5 g/25 mL, indicating reduced driving forces and clustering of the active sites at higher adsorbent concentrations. On the other hand, the removal efficiency simultaneously increases and reaches its maximum value of 98% at 0.5 g/25 mL due to the surplus surface sites, which can almost completely capture all the CIP molecules from the solution. This dual trend clearly explains the inherent trade-off between optimizing the adsorption capacity and achieving nearly complete removal of pollutants; hence, lower dosages improve the adsorption capacity on a per-gram basis but higher dosages are more effective in thoroughly removing CIP, wherein 0.5 g/25 mL is recognized as the optimal dosage for balancing removal efficiency with stability in practical applications.

3.2.3. Effect of original concentration. The effect of initial CIP concentration on the adsorption capacity (q_e, mg g^{-1}) and removal efficiency (%) of the Co/Al-LDH–CS/PVDF nanofiber membrane is shown in Fig. 6(d). It can be seen that with an increase in the original CIP concentration from 34.4 to 432 mg L^{-1}, the adsorption capacity increased from 39.1 to 352.6 mg g^{-1}, indicating that as the pollutant concentration increases, there is a greater driving force for mass transfer and

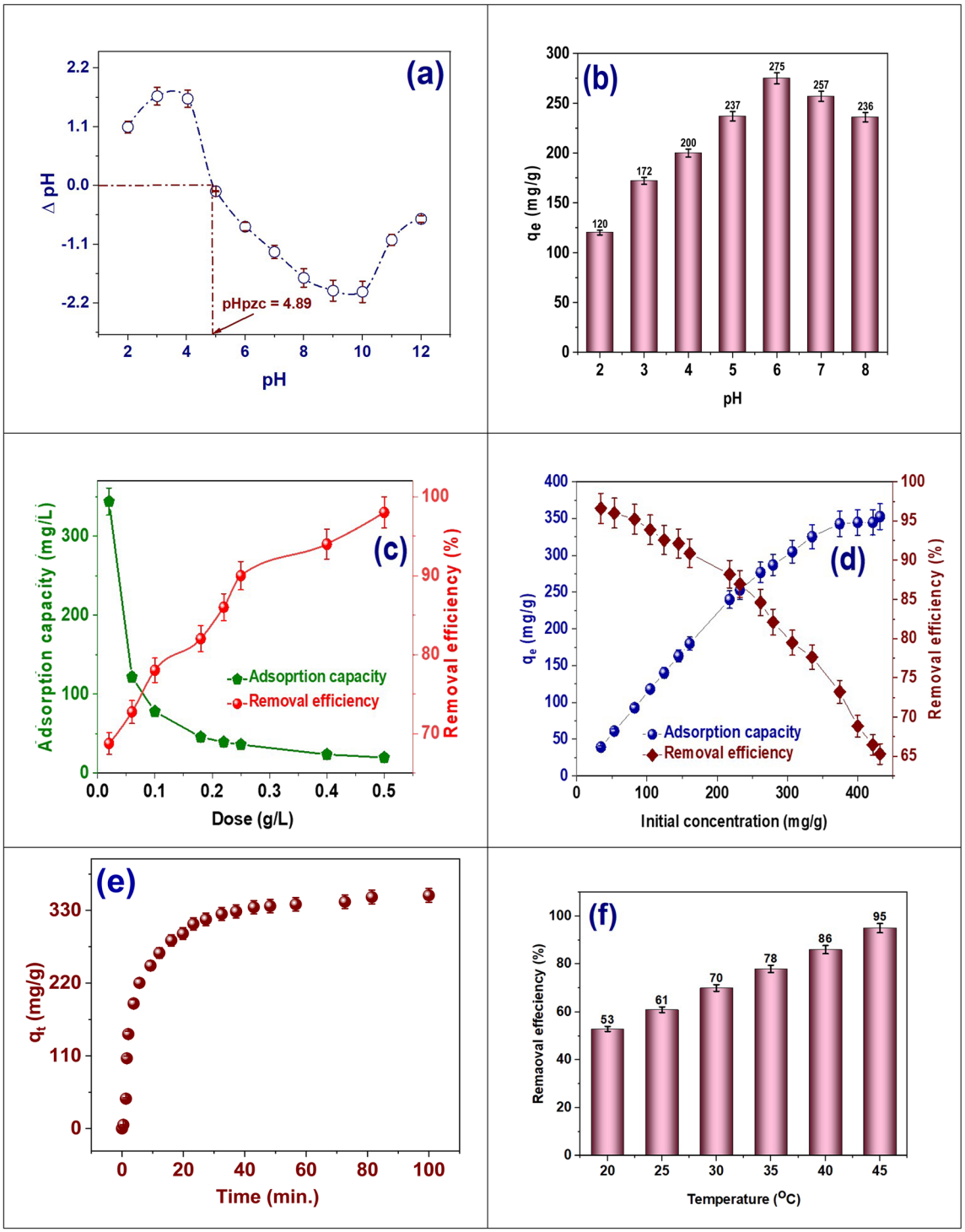

Fig. 6 (a) Determination of point of zero charge of Co/Al-LDH–CS/PVDF. (b) Effect of pH, (c) effect of adsorbent dose, (d) effect of original concentration, (e) effect of contact time, and (f) effect of temperature on the adsorption process.

easier access to readily available active sites. On the other hand, the removal efficiency decreased from 96.6% at 34.4 mg L^{-1} to 65.3% at 432 mg L^{-1}; this can be explained by the saturation of the adsorption sites at higher concentrations, where there is no sufficient surface area available for all the CIP molecules in solution even though q_e increases. At lower concentrations, there is an optimal ratio between available active sites and solute molecules allowing for near-complete removal, while at higher concentrations, it becomes site-limited yet still achieves the maximum capacity per gram of adsorbent. These results confirm that low concentration favors a high removal efficiency but high concentration favors a high adsorption capacity.[45]

3.2.4. Effect of contact time. Fig. 6(e) shows the effect of contact time on CIP adsorption on the Co/Al-LDH–CS/PVDF membrane. The adsorption capacity (q_t, mg g^{-1}) increased rapidly at first, and then reached a plateau value, indicating equilibrium. In the initial 20 min, q_t increased significantly, exceeding 280 mg g^{-1}. This rapid increase is due to the large number of active sites available on the surface of the membrane and the high concentration gradient between the solution and adsorbent. After that time, as the contact time increased beyond 20–30 min, the adsorption rate started to decline, and gradually approached an asymptote at about 330 mg g^{-1} after around 40 min. This behavior suggests that most of the available adsorption sites were already occupied and intraparticle diffusion became the rate-limiting. No further substantial increase in adsorption capacity was observed beyond this period; thus, equilibrium was reached. This kinetic pattern further confirms the high efficiency of the Co/Al-LDH–CS/PVDF nanofiber membrane with very fast uptake of CIP within a short duration, which is an advantageous feature for wastewater treatment processes demanding the swift removal of contaminants.[46]

3.2.5. Effect of temperature. The effect of temperature on the removal efficiency of CIP using the Co/Al-LDH–CS/PVDF membrane is shown in Fig. 6(f). An increased trend in elimination efficiency with an increase in temperature was significantly observed. At 20 °C, the efficiency was low (53%), which indicates restricted molecular movement and slow diffusion rates of CIP molecules toward the surface of the membrane. As the temperature increased, the removal efficiency improved from 61% at 25 °C to 70% at 30 °C, and further to 78% at 35 °C. A further increase in temperature up to 40 °C, and then to 45 °C gave even higher efficiencies, namely 86% and 95%, respectively. This trend suggests that the adsorption mechanism is endothermic; higher temperatures increase the kinetic energy and mobility of the CIP molecules, reduce the boundary layer resistance, and facilitate the diffusion of CIP into the pores of the nanofiber membrane. High temperatures could also enhance adsorption by strengthening bonds with the Co/Al-LDH active sites such as H-bonding, electrostatic attraction, and coordination. These results not only confirm that adsorption is dependent on temperature but also suggest that a small increase in temperature may enhance the CIP removal efficiency under practical conditions, emphasizing the thermodynamic favorability of this system.[47]

3.3. Adsorption isotherm

The use of different adsorption isotherm models helps in better understanding the mechanisms and efficiency of CIP removal by the Co/Al-LDH–CS/PVDF nanofiber membrane, as each model has its own advantages. The Langmuir isotherm is especially important, given that it controls the maximum adsorption capacity (q_m) and assumes that adsorption takes place on a single layer at homogenous sites.[48] Also, it gives the separation factor (R_L), which is important for judging how favorable the adsorption method is and predicting how the adsorbent will act under specific conditions. In contrast, the Freundlich model gives information about surface diversity and multilayer adsorption. Its constants (K_F and n) provide insights into the strength and spread of the adsorption sites, showing the natural complexity of uneven nanofiber surfaces.[49] The Dubinin–Radushkevich model (D–R) further clarifies the nature of adsorption. The mean free energy (E_a) from this model helps to determine whether the adsorption process is governed by weak physical forces or strong chemical interactions. This distinction is crucial in evaluating binding strength, stability, and reusability.[50] The Temkin isotherm, taking into account the interactions between the two adsorbed species, adds a further dimension to the study, and thus provides a more realistic description of the energy changes involved in the adsorption process by demonstrating that the heat of adsorption decreases with an increase in surface coverage.[51] Finally, the Jossens isotherm supports this by quantifying the affinity of the adsorbent with its K value and heterogeneity with the J parameter, confirming both the strong binding capacity and uniformity of active sites in the composite membrane. All these models work together to allow a complete evaluation of adsorption capacity, heterogeneity, energy dynamics, and site affinity, thus proving the high efficiency, stability, and mechanism dominated by chemisorption for the Co/Al-LDH–CS/PVDF membrane in treating pharmaceutical wastewater (Fig. 7(a)).

The process for the adsorption of CIP on the Co/Al-LDH–CS/PVDF membrane fits well with the Langmuir isotherm model, which describes monolayer adsorption on a homogeneous surface with equivalent active sites. The close match between the experimental value of maximum adsorption capacity (q_m, exp. = 352.6 mg g^{-1}) and theoretical values indicates that the nanofiber surface provides abundant and energetically favorable sites for CIP uptake.[48] The Langmuir constant (K_L = 0.0446 L mg^{-1}) indicates the strong affinity of the membrane for CIP, and the dimensional separation parameter (R_L = 0.48) in the range of 0–1 unambiguously confirms that adsorption is favorable over the entire concentration range studied (Table S4). The mechanism of adsorption predominantly involves electrostatic interactions between protonated functional groups of CIP and negatively charged hydroxyl as well as amino sites on chitosan/LDH at pH values above pH_{zpc} (4.89), which are further supplemented by hydrogen bonding, metal–ligand coordination with the Co and Al centers, π–π stacking or interactions between fluorine from PVDF matrix and the quinolone ring of CIP. The Langmuir isotherm curve shows a rapid increase in adsorption capacity at lower CIP concentrations before leveling off at higher ones; this suggests that the sites become saturated, leading to monolayer coverage (Table S5).

The adsorption behavior of CIP on the Co/Al-LDH–CS/PVDF membrane was analyzed using the Freundlich isotherm model. This model is based on a heterogeneous surface capable of multilayer adsorption and an exponential distribution of adsorption energies over the temperature range studied. The high Freundlich constant value (K_F = 59.03 mg g^{-1} (L mg^{-1})$^{1/n}$) indicates that this membrane has significant adsorption capacity and strong affinity towards CIP molecules.[49] The heterogeneity factor is 2.65, which is greater than 1. This implies that adsorption is very effective and that the nanofiber membrane has different types of surface sites with different

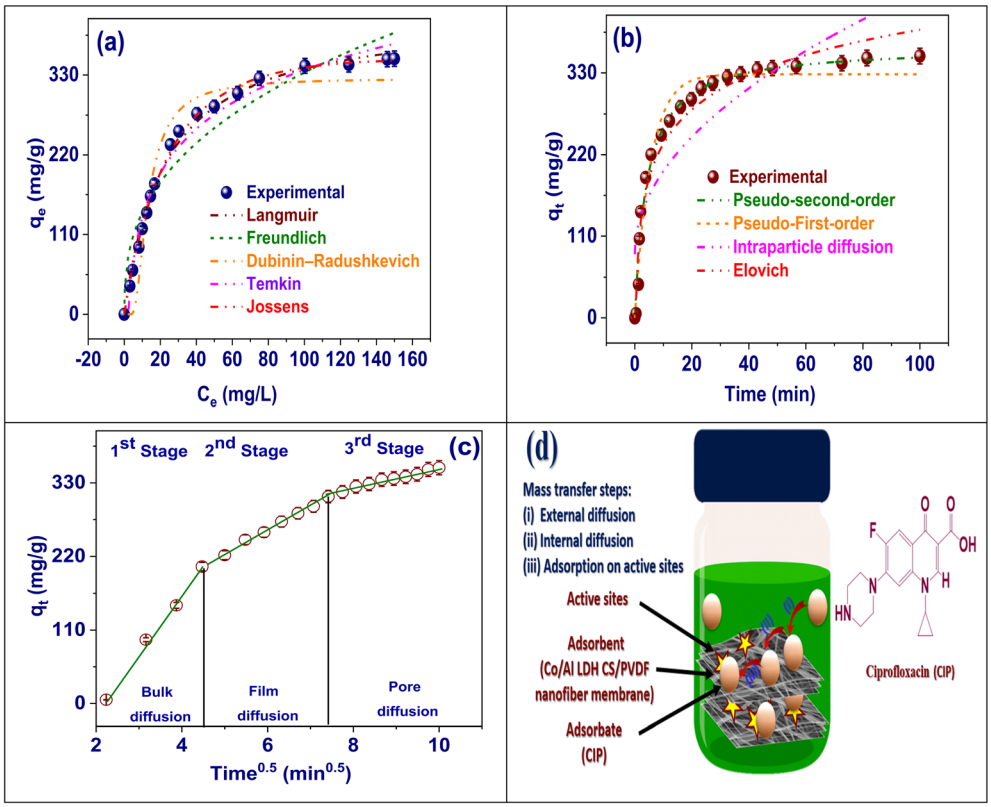

Fig. 7 (a) Models of the adsorption isotherms of Co/Al-LDH–CS/PVDF. (b) Models of the adsorption kinetics of Co/Al-LDH–CS/PVDF. (c) IPD model, and (d) schematic of the diffusion of CIP in Co/Al-LDH–CS/PVDF.

energies for catching pollutants. These findings suggest that besides monolayer adsorption described by the Langmuir model, multilayer adsorption and interactions happening at sites with different energy levels are also important contributors to the total adsorption. The large value of n also implies that there is a good distribution of adsorption sites, which corresponds with the various functional groups present in the Co/Al-LDH–CS/PVDF system, which contains hydroxyl and amino groups from chitosan, active metal centers from LDH and fluorine-rich PVDF areas, providing several binding pathways. Therefore, the Freundlich model best describes the complex and heterogeneous nature of CIP adsorption, confirming that the membrane surface supports multilayer coverage with various interaction mechanisms, thus enhancing its efficiency for the removal of pharmaceuticals.

The Dubinin–Radushkevich isotherm model was used to analyze the adsorption of CIP on the Co/Al-LDH–CS/PVDF, which helps understand the adsorption mechanism and type of interactions involved.[50] The maximum adsorption capacity obtained from the D–R model (Q_{DR}) was found to be 325.35 mg g^{-1}. This value is in good agreement with that determined from the Langmuir and Freundlich isotherm models, further confirming the strong adsorption performance of the membrane. The D–R constant ($K_{DR} = 2.27 \times 10^{-5}$ mol^2 kJ^{-2}) reflects the porosity and energy distribution over the adsorbent surface, indicating that stronger interactions are involved in the adsorption mechanism rather than purely physical ones. In addition, the mean free energy of adsorption (E_a) was calculated to be 31.8 kJ mol^{-1}, which exceeds the common threshold of 8 kJ mol^{-1} for physisorption, representing that chemisorption is the major process taking place. The high E_a value indicates that CIP adsorption is influenced by chemical bonding such as electrostatic attraction, hydrogen bonding, and coordination with the Co and Al active centers instead of van der Waals forces. These results support that Co/Al-LDH–CS/PVDF promotes an adsorption pathway dominated by chemisorption, which enhances its stability, selectivity, and efficiency toward the removal of pharmaceutical pollutants.

The Temkin adsorption isotherm was applied to study the interaction between CIP and Co/Al-LDH–CS/PVDF concerning adsorbate–adsorbent interaction characteristics and heat of adsorption. The Temkin constant ($b_T = 27.928$ J mol^{-1}) reveals that the process of adsorption is somewhat energetic, implying that due to the repulsion between the adsorbent and adsorbate, the heat of adsorption decreases linearly with an increase in surface coverage. This indicates that the process of adsorption involves not only physical but also certain interactions between CIP molecules and the functional groups present in the composite membrane such as hydrogen bonding and electrostatic attraction. In addition, the binding constant at equilibrium ($K_T = 0.45$ L mol^{-1}) reflects a favorable binding affinity, which further confirms the strong ability of the Co/Al-LDH–CS/PVDF membrane to effectively capture CIP from aqueous solutions. All these results indicate that the Temkin model well

describes the heterogeneous nature of the adsorption sites, along with the adsorbate–adsorbent interaction effects, thereby confirming the energetically favorable, efficient, and mainly chemisorption-driven mechanism of CIP adsorption on the nanofiber membrane.

The adsorption isotherm of CIP on the Co/Al-LDH–CS/PVDF nanofiber membrane was fitted with the Jossens model. This isotherm is mainly applied in heterogeneous adsorption systems with variable energies at different sites. The computed Jossens constants were $K = 15.015$ and $J = 0.017$, which provide good insight into the possible adsorption mechanisms. The relatively high value of K indicates strong attraction between the membrane and the CIP molecules, emphasizing its ability to capture pharmaceutical contaminants even at low concentrations. On the other hand, the very small value of J indicates the low heterogeneity of the adsorption sites; hence, although the membrane surface is not completely uniform, the differences in site energy are low and lead to uniformity in adsorption behavior. Most of the active sites on the composite nanofiber are probably energetically similar, and thus they can interact strongly with CIP by electrostatic force, H-bonding, and coordination with the Co/Al active centers. The results from this model support the efficiency and reliability of Co/Al-LDH–CS/PVDF having a high binding affinity together with a fairly uniform adsorption surface for achieving consistent reproducible CIP removal from aqueous systems.

The adsorption isotherm study of CIP on the Co/Al-LDH–CS/PVDF composite material revealed its high affinity and capacity for adsorption through several model validations. The Langmuir model provided an excellent fit with monolayer adsorption at uniform sites having a favorable affinity, as indicated by the experimental capacity (352.6 mg g^{-1}) and parameters K_L = 0.0446 L mg^{-1} and $R_L = 0.48$. The Freundlich model suggested surface heterogeneity and multilayer adsorption with a heterogeneity factor $n = 2.65$, which is more than one, confirming favorable conditions of adsorption, along with a high Freundlich constant $K_F = 59.03$ mg g^{-1} (L mg^{-1})$^{1/n}$ reflecting a strong binding strength. In addition, the Dubinin–Radushkevich model estimated the maximum adsorption capacity of 325.35 mg g^{-1} and energy of adsorption $E_a = 31.8$ kJ mol^{-1}, which is above the threshold for physical adsorption, indicating the participation of chemical adsorption aided by electrostatic forces, hydrogen bonding, and coordination to the Co/Al active sites.[51] The Temkin model further confirmed the importance of interactions between the adsorbate and adsorbent with a moderate adsorption energy ($b_T = 27.928$ J mol^{-1}) decreasing with increasing surface coverage and a favorable binding process given by $K_T = 0.45$ L mol^{-1}. Finally, the Jossens model supported this finding with a high affinity constant ($K = 15.015$) and low heterogeneity parameter ($J = 0.017$), meaning that most of the adsorption sites have similar energy levels, resulting in a uniform and reproducible adsorption performance. The results from the isotherm models in general prove that the adsorption of CIP on Co/Al-LDH–CS/PVDF is effective, efficient, and mainly chemisorption-based through different mechanisms involving monolayer–multilayer interactions over various surface sites, making this membrane a good candidate adsorbent for pharmaceutical wastewater treatment.

The isotherm parameters summarized in Table S5 reveal a significant enhancement in the adsorption of CIP on the Co/Al-LDH–CS/PVDF membrane. The Langmuir model shows that the Co/Al-LDH–CS/PVDF membrane has a higher maximum adsorption capacity (q_m, exp. = 352.6 mg g^{-1}) than the unmodified CS/PVDF membrane (289.8 mg g^{-1}), further confirming that the LDH plays an important role in increasing the number of available sites for adsorption. Both systems have good adsorption behaviors ($0 < R_L < 1$), but the LDH-modified membrane has a greater surface affinity for CIP. This is confirmed by the Freundlich parameters, where the Co/Al-LDH–CS/PVDF membrane has a better K_F value (59.03 mg g^{-1} (L mg^{-1})$^{1/n}$) than that of the CS/PVDF membrane (47.92 mg g^{-1} (L mg^{-1})$^{1/n}$). This indicates an increase in adsorption intensity, with similar n values (>2) for both membranes, which reflect favorable adsorption on heterogeneous surfaces. The Dubinin–Radushkevich model shows a higher theoretical adsorption capacity ($Q_{DR} = 325.35$ mg g^{-1}) and mean adsorption energy (E_a = 31.8 kJ mol^{-1}) for the LDH membrane than the CS/PVDF membrane (Q_{DR} = 266.92 mg g^{-1} and E_a = 29.84 kJ mol^{-1}), which indicates increased chemisorption due to the presence of Co/Al-LDH. Additionally, the Temkin and Jossens parameters give higher interaction constants of b_T, K_T, and K for the Co/Al-LDH–CS/PVDF membrane, which means better adsorbate–adsorbent interactions and binding affinity towards CIP. In summary, the addition of Co/Al-LDH in the CS/PVDF membrane increases its adsorption capacity as well as interaction strength and energetic favorability, which is a significant advantage in terms of efficiently removing ciprofloxacin from water solutions (Fig. S1(a)).

3.4. Adsorption kinetics

The use of adsorption kinetic models in the study of the rate, mechanism, and controlling factors of CIP uptake on the Co/Al-LDH–CS/PVDF nanofiber membrane offers great benefits given that they provide important information necessary for understanding its fundamental mechanisms as well as practical optimization. The pseudo-first-order model is applicable for defining adsorption processes where the rate of solute uptake is directly related to the concentration of unoccupied active sites, which suggests that the initial binding may be limited to the surface.[52] The pseudo-second-order model indicates that the adsorption process is influenced by chemisorption involving valence forces through sharing or exchange of electrons between the CIP particles and active sites on the nanofiber membrane. This model usually fits better with experimental data because it incorporates stronger interactions such as electrostatic attraction, H-bonding, and coordination with the Co/Al centers. The intraparticle diffusion model determines if the diffusion of CIP particles into the pores of the nanofiber matrix is the rate-limiting step.[53] Typically, this is found in multi-step adsorption processes, where fast surface adsorption happens before a slower diffusion process in the porous material continues until equilibrium is reached. On the other hand,

the Elovich model is more appropriate for systems with different surface energies given that it reflects chemisorption on energetically heterogeneous sites and provides insight into surface activation and gradual site saturation. By applying these kinetic models, one can distinguish between physisorption and chemisorption, assess the relative importance of surface *versus* diffusion control, and fully appreciate how adsorption changes with time. Thereby, the results confirm that CIP adsorption on the Co/Al-LDH–CS/PVDF nanofiber membrane proceeds quickly and mainly through chemisorption, with significant influences from pore diffusion and surface heterogeneity (Table S4).

The kinetic studies of CIP adsorption on the Co/Al-LDH–CS/PVDF membrane commenced with the pseudo-first-order model, which presumes that the rate of adsorption is proportional to the number of available active sites. The rate constant obtained ($K_1 = 0.18 \times 10^{-2}$ min^{-1}) under this model suggests a rather slow adsorption process, thus confirming the inadequacy of this model to describe the fast and strong interaction nature of CIP with the nanofiber composite.[52] The pseudo-first-order equation is generally applicable to systems controlled by physisorption, which involves weak van der Waals interactions; however, the lower fitting accuracy of this equation compared to the other models suggests that physisorption may not be the primary mechanism of adsorption in this case.[54] Rather, the differences between the results from the experiments and that predicted by the pseudo-first-order model suggest that chemisorption mechanisms might be more important (Table S6). However, it is good to use this model because it provides a basis for comparison to distinguish the contributions from physical and chemical adsorption. This confirms that CIP interacts with Co/Al-LDH–CS/PVDF through stronger forces than simple surface physisorption (Fig. 7(b)).

The process of CIP adsorption on the Co/Al-LDH–CS/PVDF membrane can be best described by the pseudo-second-order kinetic model. This model assumes that adsorption is controlled by chemisorption through interactions such as valence forces, exchange of electrons, or sharing of electrons between the adsorbate and adsorbent. The rate constant obtained ($K_2 = 6.4 \times 10^{-4}$ g mg^{-1} min^{-1}) indicates that adsorption takes place at a slower rate than physical adsorption but shows greater strength and stability in the binding mechanism. The equilibrium adsorption capacity predicted by this model (q_e = 355.45 mg g^{-1}) is very close to that obtained experimentally, thus validating its application in describing the kinetics of CIP adsorption.[54] The strong correlation indicates that adsorption mainly occurs through chemisorption, governed by the electrostatic interaction between protonated CIP species and the membrane surface at $pH_{zpc} = 4.89$, with some involvement of hydrogen bonding and coordination to the active Co/Al sites in the nanofiber matrix. Therefore, while the pseudo-second-order model provides an adequate fit to the experimental data, supporting its validity as an accurate estimate of adsorption capacity, it also indicates that chemical interactions are the primary rate-controlling step for CIP immobilization on Co/Al-LDH–CS/PVDF.

The intraparticle diffusion model would provide greater insight into the adsorption kinetics of CIP on Co/Al-LDH–CS/PVDF in terms of whether pore diffusion could be a limiting factor in the process.[53] The calculated intraparticle diffusion rate constant K_i (35.37 mg g^{-1} min$^{-1/2}$) suggests that CIP molecules diffuse relatively fast into the porous structure of the membrane. The value of the intercept (X = 85.80 mg g^{-1}) also indicates that boundary layer effects are important and control the rate of adsorption (Fig. 7(c)). In fact, this straight-line plot does not pass through the origin, which means that surface adsorption processes occur together with intraparticle diffusion as the mechanism controlling the rate. This behavior due to the high availability of active sites reflects an initial stage of fast adsorption on the exterior surfaces and a longer one where CIP particles move inside the internal pores of the nanofiber membrane until equilibrium is reached; hence, the intraparticle diffusion model emphasizes pore diffusion plus surface binding, confirming that although interparticle transport plays an important part in the overall adsorption, it is governed by both surface interactions and slow molecular transfer within the porous networks (Fig. 7(d)).

The Elovich kinetic model was used to analyze CIP adsorption on the Co/Al-LDH–CS/PVDF nanofiber membrane. This model is most applicable when there are highly heterogeneous surfaces and chemisorption is the main mechanism. The initial adsorption rate (α = 0.05 mg g^{-1} min^{-1}) denotes the moderate uptake of CIP, which agrees with many active sites being available at the beginning of the procedure. The desorption constant (β = 66.67 g mg^{-1}) indicates that as adsorption proceeds, the rate drops significantly due to site saturation and an increase in activation energy needed for CIP molecules to get to the other less energetically favorable sites.[55] This pattern aligns with the rapid adsorption phase observed initially, which was explored using a gradual approach to reach equilibrium in batch experiments. A benefit of the Elovich model is its capability to represent adsorption processes on surfaces that have different energy characteristics, such as the Co/Al-LDH–CS/PVDF composite material, which contains a combination of hydroxyl, amino, and metal-active sites as well as domains of fluorinated PVDF. The results confirm that CIP uptake is predominantly chemisorption driven; it occurs first on the high-energy active sites, and then gradually shifts to low-energy ones. This behavior describes the heterogeneous and multifunctional nature of the composite nanofiber membrane.[55]

The Co/Al-LDH–CS/PVDF nanofiber membrane exhibited greatly enhanced adsorption kinetics for CIP when compared to the original membrane. The pseudo-second-order kinetic model, which indicates that chemisorption is the main mechanism for both membranes, further confirms that the Co/Al-LDH–CS/PVDF membrane has a better equilibrium capacity (q_e = 355.45 mg g^{-1}) than the CS/PVDF membrane (291.6 mg g^{-1}). This is in accordance with the experimental data and emphasizes the role of LDH in increasing the number of chemically reactive sites. Although the pseudo-first-order rate constants (K_1) for both membranes are approximately equal, their lower values indicate that physical adsorption cannot fully account for the dynamic adsorption observed (Table S6). A higher diffusion rate constant was determined from the intraparticle diffusion model for the LDH-modified membrane (K_i = 35.37 mg g^{-1}

$min^{-1/2}$) than for the CS/PVDF membrane (26.38 mg g^{-1} $min^{-1/2}$), which means that CIP transfers into its porous structure faster due to its mesopores induced by LDH. The larger intercept value ($X = 85.80$ mg g^{-1}) of the Co/Al-LDH–CS/PVDF membrane indicates the involvement of a more significant boundary-layer effect and higher surface adsorption initially. Moreover, the Elovich model parameters favor enhanced chemisorption given that the LDH-containing membrane shows a higher initial adsorption rate (α = 0.05 mg g^{-1} min^{-1}) and larger β value, indicating stronger adsorbate–adsorbent interactions and greater activation energy requirements. Hence, it can be concluded that the incorporation of Co/Al-LDH into the CS/PVDF membrane accelerated the adsorption rate, improved diffusion, and enhanced chemisorption interactions, resulting in a considerable kinetic advantage for removing ciprofloxacin from water (Fig. S1(b)).

3.5. Diffusion mechanism

Intraparticle diffusion kinetics of CIP adsorption on Co/Al-LDH–CS/PVDF nanofiber membrane is divided into three stages as shown in the Fig. 7(c): bulk diffusion, film diffusion, and pore diffusion. These steps are associated with different rate-controlling mechanisms. In the first phase, which is bulk diffusion, an increase in adsorption capacity is observed due to fast CIP particle transport from the main solution to the external surface of the nanofiber membrane.[53] This process is governed by a significant concentration gradient and abundance of available adsorption sites (Fig. 7(d)). The second stage, film diffusion, refers to the movement of CIP molecules through the boundary layer surrounding the nanofiber surface. In this phase, the rate of adsorption becomes slower as the molecules have to pass through this resistance zone before they can start interacting with the functional groups such as hydroxyl, amino, and metal sites in Co/Al-LDH–CS/PVDF. Pore diffusion is the last step, which signifies the unimpeded transport of CIP into the internal porous structure of the membrane. At this point, adsorption increasingly becomes limited by steric hindrance and a reduction in available active sites until it reaches an equilibrium concentration of about 330 mg g^{-1}. The multilinear nature of the plot and the fact that it does not pass through the origin suggest that intraparticle diffusion is not only controlling but rather working together with surface adsorption and film transfer mechanisms. In general, this three-stage diffusion behavior means that the adsorption of CIP is controlled somehow by fast outside adsorption, middle film diffusion, and slow inner particle diffusion, confirming the good and complex uptake behavior of the Co/Al-LDH–CS/PVDF membrane.

3.6. Thermodynamics

Increasing temperature enhances the uptake of CIP on the Co/Al-LDH–CS/PVDF membrane, and the thermodynamic and kinetic parameters that govern this process are fully discussed. According to the van't Hoff plot (Fig. 8(a)), ΔH^0 was determined to be +83.62 kJ mol^{-1} and ΔS^0 was found to be +282.65 J mol^{-1} K^{-1}, indicating that the process is endothermic and becomes more favorable with increasing temperature.[56] The positive ΔS^0 indicates that interfacial disorder increased and this contributes to a more favorable "fit" and greater freedom of CIP molecules on the surface and within the pores. Thus, ΔG^0

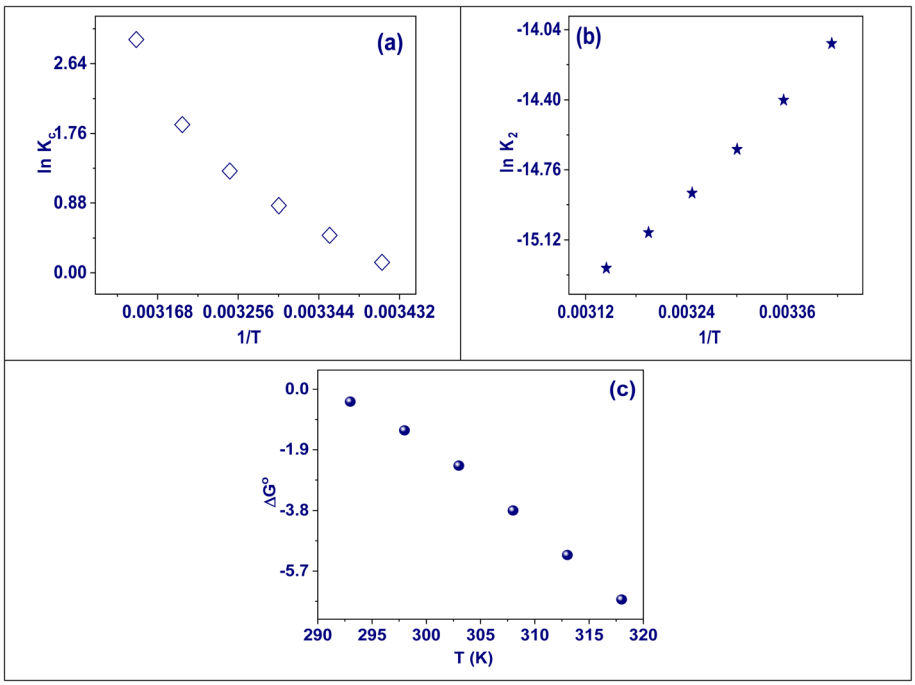

Fig. 8 Effect of temperature on the adsorption of CIP onto Co/Al-LDH–CS/PVDF *via* (a) van't Hoff plot, (b) Arrhenius plot, and (c) effect of temperature on ΔG^0.

changes from a slightly negative value at 293 K (−0.39 kJ mol^{-1}) to gradually more negative values at 298, 303, 308, 313, and 318 K, reaching −6.59 kJ mol^{-1} (Fig. 8(b)). This means that the spontaneity increases with temperature.[57] The reason for this is that the term $T\Delta S^0$ starts to dominate in the equation for the Gibbs free energy ($\Delta G^0 = \Delta H^0 - T\Delta S^0$). The Arrhenius study provides an activation energy, E_a, of 36.82 kJ mol^{-1}, which indicates a fairly high energy barrier. This matches with reactions on surfaces or complexation aided by temperature and more movement through both the film and the spaces inside particles (see Fig. 8(c)). From a practical viewpoint, increasing the temperature decreases the solution viscosity, which improves the mobility of the CIP molecules, helps in overcoming mass-transfer resistance, and can activate or generate adsorption sites in Co/Al-LDH–CS/PVDF (refer to Table S7). Thus, both the adsorption capacity and rate are enhanced by temperature, consistent with the positive ΔH^0, and further negative ΔG^0. Therefore, this process is described as endothermic with an entropy-driven mechanism that becomes more spontaneous at higher temperatures.[58]

3.7. Mechanism of interaction

In considering the factors related to adsorption, it is important to speculate on a number of possible problems that may influence the effectiveness of this process. In general, the adsorption phenomenon is governed by the structural characteristics of both the adsorbent and adsorbate. Different functional groups, especially –OH groups, are instrumental in controlling the interaction between CIP and the Co/Al-LDH–CS/PVDF membrane surface. By studying them separately, one can gain some understanding regarding the possible mechanisms of adsorption taking place over the Co/Al-LDH–CS/PVDF membrane. (i) Electrostatic attraction can be defined here as an interaction between surfaces with opposite electrical charges.[18] The nature of the interaction will depend on the charge of the contaminant and the pH of the solution. Given that the Co/Al-LDH–CS/PVDF membrane has a point of zero charge of 4.89, this means that at low pH, the functional groups on the membrane are protonated and that Co/Al-LDH–CS/PVDF carries a positive charge. This indicates that there may be some electrostatic attraction between the positively charged sites on the surface of the membrane and CIP. (ii) The main mechanism involved in dipole–dipole interaction is commonly referred to as hydrogen bonding. It occurs when two atoms participate in an interaction where one atom acts as a donor of hydrogen and another atom becomes an acceptor.[29] In this case, the hydrogen acceptors are supplied by CIP and consist mostly of atoms of oxygen and nitrogen. The hydrogen donor is expected to come from the –OH groups of the magnetite elements provided by Co/Al-LDH–CS/PVDF. The strength of hydrogen bonding has a direct relation with the number of hydrogen atoms present in the Co/Al-LDH–CS/PVDF membrane. It also relies on whether there are any oxygen and/or nitrogen atoms in the molecule in question. (iii) The phenomenon of pore blockage could be one reason behind drug adsorption on the Co/Al-LDH–CS/PVDF membrane, as evidenced by the significant decrease in its surface area, pore diameters, and adsorption capacity before and after an adsorption event.[59,60] This observation indicates that some of the CIP was taken in by the pores of the adsorbent; it could also happen at the same time as ion exchange, as shown in Fig. 9.

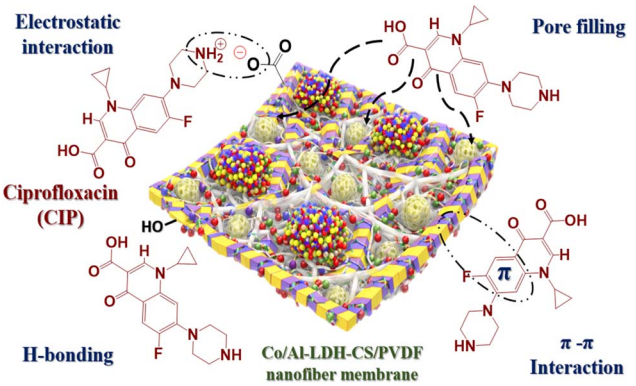

Fig. 9 Schematic of the contact interaction mechanism between CIP and Co/Al-LDH–CS/PVDF.

3.8. Result of salinity

The effect of anions including Cl^-, SO_4^{2-}, NO_3^-, and HCO_3^- on the adsorption capacity of Co/Al-LDH–CS/PVDF for CIP was tested at an initial CIP concentration of 200 mg L^{-1} and a salt concentration of 50 mg L^{-1}. As shown in Fig. 10, chloride ions have an insignificant effect on CIP adsorption with a maximum removal efficiency of 92.2%. Sulfate and nitrate ions have a slight effect on CIP adsorption; in fact, SO_4^{2-} resulted in a removal efficiency of only 80.6%, which is further reduced to 84.2% in the presence of NO_3^-.[61] In contrast, the presence of HCO_3^- ions greatly inhibited the removal of CIP, with a reduction in removal efficiency to just 68.8%. A higher pH could lead to more deprotonation on the adsorbent surface, resulting in lower adsorption due to repulsive forces. The findings indicate

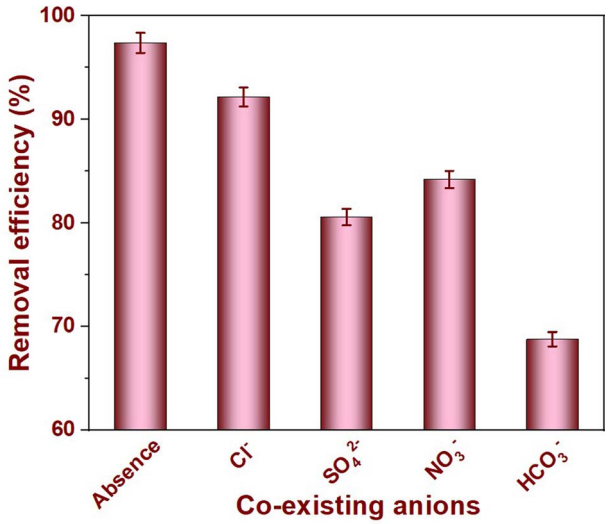

Fig. 10 Result of the effect of salinity on the adsorption of CIP onto Co/Al-LDH–CS/PVDF.

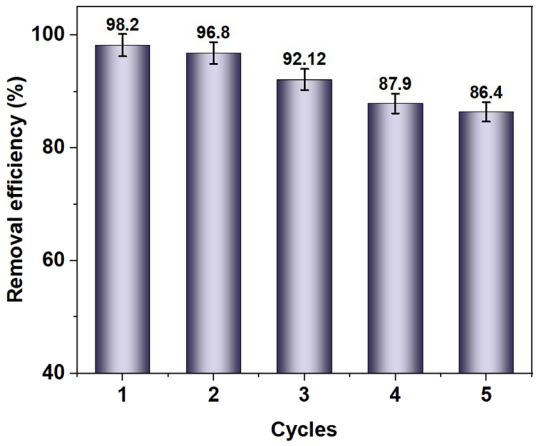

Fig. 11 Cycles of reusability for the Co/Al-LDH–CS/PVDF membrane.

that CIP competes for active sites on the Co/Al-LDH–CS/PVDF membrane surface with Cl^-, SO_4^{2-}, NO_3^-, and HCO_3^- ions.

3.9. Reusability

In the reusability experiment, 50 mL of aqueous solution containing ciprofloxacin (CIP) at a concentration of 100 mg L^{-1} was treated with 0.02 g of the Co/Al-LDH–CS/PVDF composite membrane.[62] The experiment was performed under controlled conditions with a pH of 8 and absorption time of 100 min to study the adsorption capacity for CIP. After filtration, the CIP-saturated adsorbent was eluted with a 50 mL solution of ethyl alcohol and hydrochloric acid in a volume ratio of 7 : 3 to enhance CIP desorption. The adsorbent was stirred for 30 min at 25 °C to allow the maximum interaction between the adsorbent and elution solvent. Centrifugation was then used to separate the Co/Al-LDH–CS/PVDF membrane from the mixture. After washing with distilled water, the membrane was dried at 65 °C, which is a temperature suitable for subsequent use cycles. The adsorption and reactivation processes were studied over five different intervals. The significant ability of the sorbent to withstand multiple usage cycles is a key factor highlighting its practical applicability in commercial settings. In the five-consecutive series of adsorption and desorption, there was a significant decrease in its retention capacities with values of 98.2%, 96.8%, 92.12%, 87.9%, and 86.4% of its initial capacity, showing a gradual decline. This observed decrease in capacity can be understood based on two principal reasons: the reduced availability of active sites and changes in the molecular structure of the compound, which are intensified with each cycle (Fig. 11). The results demonstrate that the Co/Al-LDH–CS/PVDF membrane has high efficiency for recycling purposes.

3.10. Comparison with other adsorbents

The assessment of the extreme sorption capacities for comparison with the values cited in the literature, as given in Table S8, is a step towards realizing a broad understanding of the effectiveness of the sorbent, notwithstanding the inherent difficulties in establishing direct correlations in findings due to the varying experimental conditions. The rapid interaction property of the Co/Al-LDH–CS/PVDF membrane as a sorbent presents another significant advantage. Its high binding capacity for CIP indicates that it may be possible to use this material for wastewater management, specifically for removing this pollutant from water.

3.11. Statistical analysis

Response surface methodology (RSM) was used to investigate, predict and optimize the effects of different independent variables on the performance of the adsorbent in removing CIP. The

Table 2 ANOVA study of the variance to assess the appropriateness of the models

Source	Sum of the squares	df	Mean square	*F*-Value	*p*-Value	
Model	1.772×10^5	9	19 687.63	45.27	<0.0001	Significant
A-pH	1856.42	1	1856.42	4.27	0.0777	
B-Dose	8533.27	1	8533.27	19.62	0.0030	
C-Time	1.183×10^5	1	1.183×10^5	271.99	<0.0001	
AB	301.96	1	301.96	0.6943	0.4322	
AC	737.67	1	737.67	1.70	0.2340	
BC	4238.01	1	4238.01	9.74	0.0168	
A^2	8790.85	1	8790.85	20.21	0.0028	
B^2	129.12	1	129.12	0.2969	0.6028	
C^2	31 848.41	1	31 848.41	73.23	<0.0001	
Residual	3044.49	7	434.93			
Lack of fit	3044.49	3	1014.83			
Pure error	0.0000	4	0.0000			
Corr. total	1.802×10^5	16				
R^2	0.9831					
Adjusted R^2	0.9614					
Predicted R^2	0.7297					
Adeq. precision	21.8958					
Std. dev.	20.85					
Mean	173.07					
C.V. (%)	12.05					

Table 3 Total squares of the successive models

Source	Sum of the squares	df	Mean square	Sequential p-value	Adjusted R^2	Predicted R^2	
Linear	51 546.15	9	5727.35	0.0008	0.6480	0.5145	
2FI	46 268.51	6	7711.42	0.7695	0.5893	0.1515	
Quadratic	3044.49	3	1014.83	0.0002	0.9614	0.7297	Suggested
Cubic	0.0000	0			1.0000		Alias

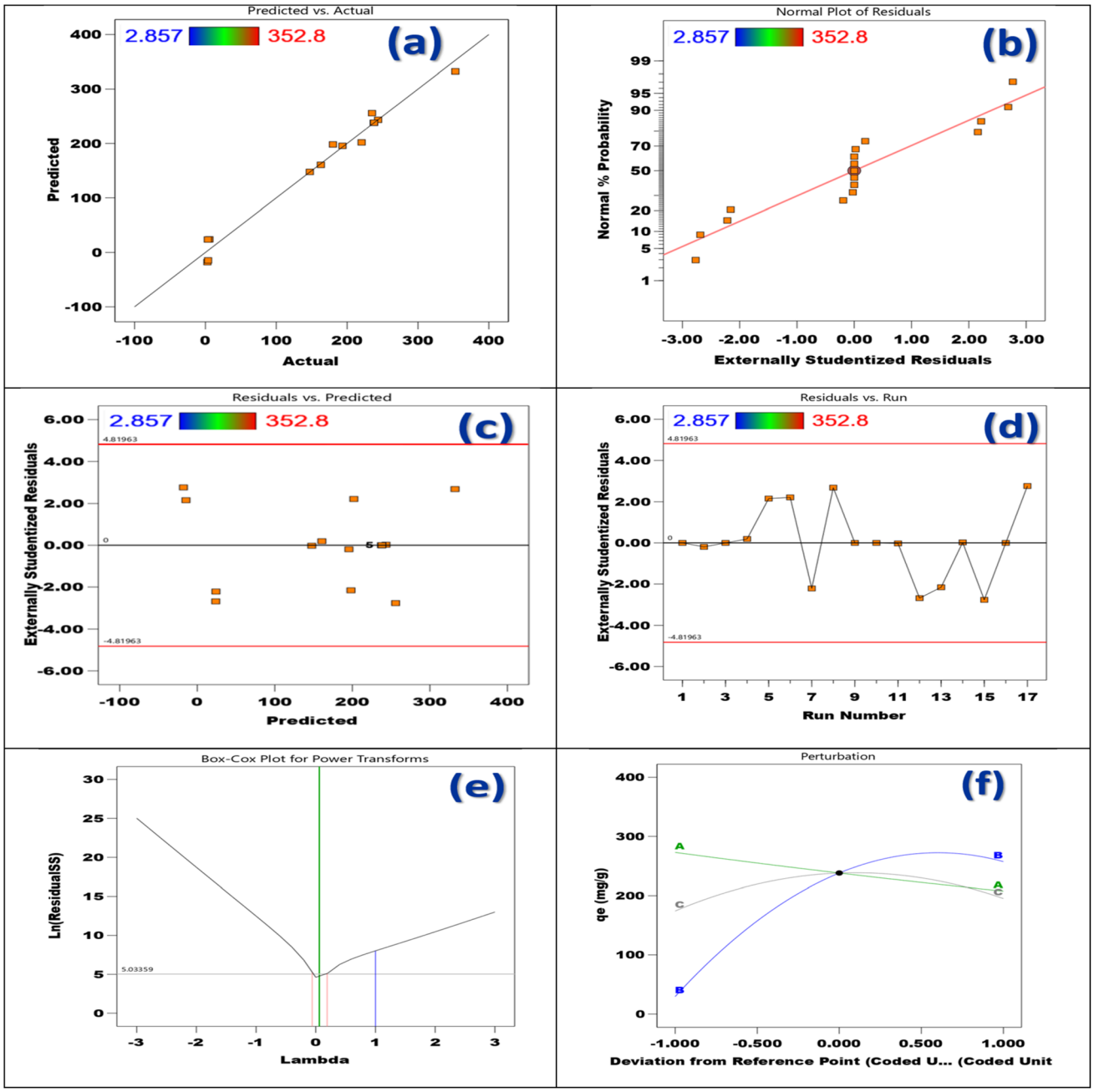

Fig. 12 (a) Actual values *versus* anticipated values, (b) standard residual prospect, (c) deviations in relation to projected values, (d) deviations compared to sequence, (e) Box–Cox plot, and (f) perturbation plot.

independent variables considered were concentration in the range of 34 to 432 mg L^{-1}, dosage of Co/Al-LDH–CS/PVDF membrane from 0.02 to 0.50 g, pH from 2 to 12, and contact time between 5 and 100 min.[63,64] The experimental design included 17 runs of 3 factors in a completely randomized design, as shown in Table 1. Besides, the ANOVA results in Table 2 point out the factors that have a significant effect on the removal process. The significance and relevance of each independent variable were determined using *F*-value and *p*-value assessments to evaluate their statistical effects.[65,66] The variables pH (*A*), amount of Co/Al-LDH–CS/PVDF membrane (*B*), and contact time (*C*) had *p*-values less than 0.05, showing that they are statistically significant and have a great effect on the removal process, as indicated in Table 2.[67,68] Model fit evaluation was performed using R^2 and adjusted R^2 metrics. In experimental studies, R^2 explains the percentage reduction in variance with respect to the response definition in the model. However, a high R^2 value does not always indicate a good fit

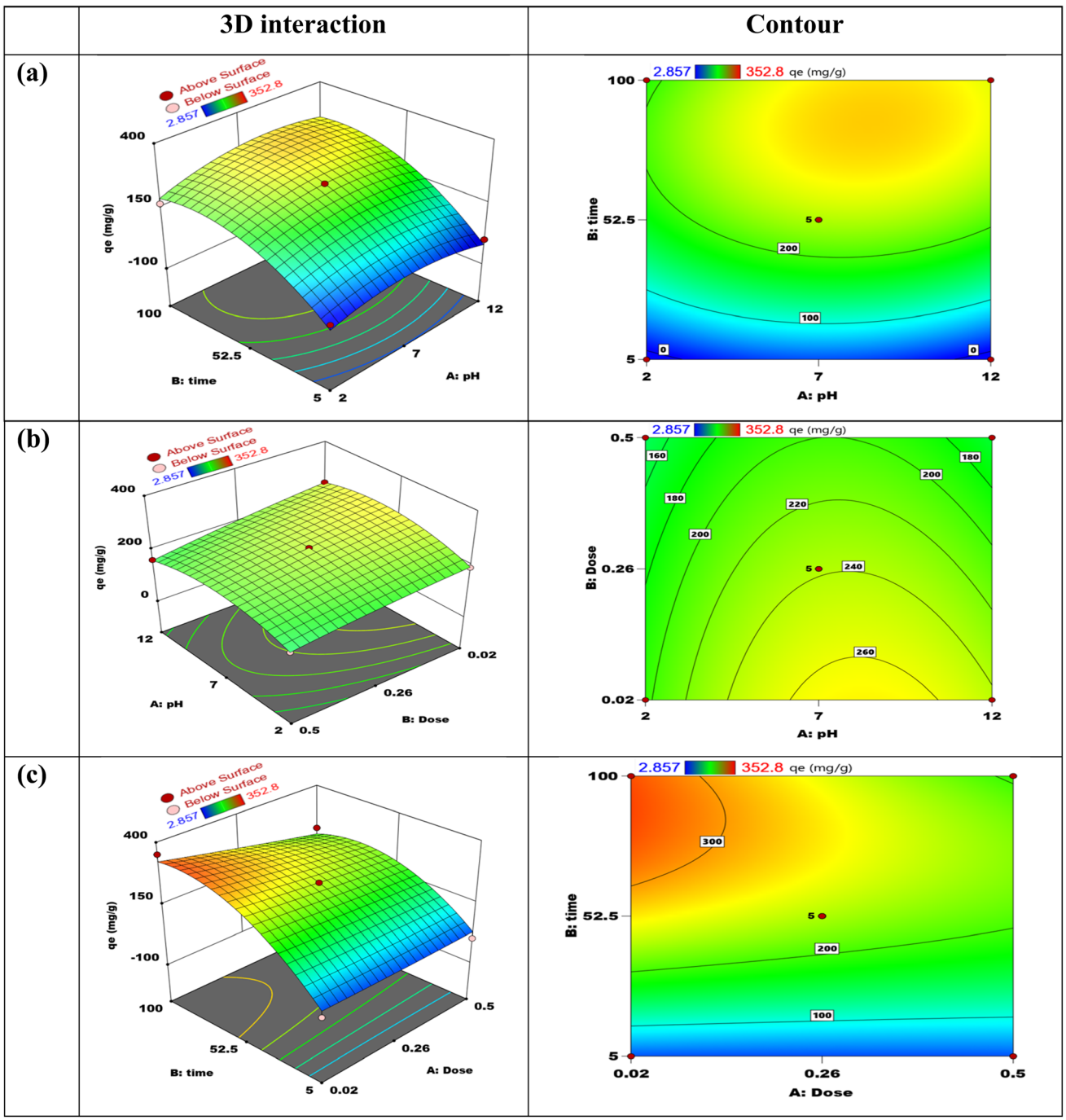

Fig. 13 Response surface of the three-dimensional and contour representations of the interactive effects of: (a) pH and contact time, (b) pH and membrane dosage, and (c) contact time and membrane dosage on the adsorption capacity of ciprofloxacin.

because it will always increase when new variables are added, regardless of whether these variables are statistically significant. Therefore, adjusted R^2 is considered a better measure given that it does not necessarily increase with the addition of more variables; in fact, the addition of irrelevant variables may reduce it. The difference between R^2 and adjusted R^2 values may be large when unnecessary variables are included in the model. In this study, the R^2 values showed an excellent 98.31% fit, while the adjusted R^2 values indicated a 96.14% fit, which means that the proposed model can be used effectively to evaluate adsorption capacity. Its importance was highlighted by its very large model F-value of 45.27; this high value would be due to chance alone with a probability of only 0.01%. A quadratic model was fitted to the data, as described in Table 3. Parameters and responses were expressed in coded values through eqn (4), while the actual equation is given in eqn (5).

$$q_e = 238.109 + 15.2333 \times A - 32.6597 \times B + 121.603 \times C - 8.6885 \times AB + 13.58 \times AC - 32.55 \times BC - 45.6928 \times A^2 - 5.53775 \times B^2 - 86.9712 \times C^2 \quad (4)$$

The equation presented in implicit factors serves as a predictive tool for estimating the effect associated with different levels of each factor. In this coded equation, high levels of the factors are traditionally represented by +1 and low levels are represented by −1. The coefficients of the factors in this coded equation provide an indication of the relative importance of the factors.

$$q_e = -115.679 + 27.5152 \times \text{pH} + 114.496 \times \text{dose} + 6.94958 \times \text{time} + -7.24042 \times \text{pH dose} + 0.0571789 \times \text{pH time} - 2.85526 \times \text{dose time} - 1.82771 \times \text{pH}^2 - 96.1415 \times \text{dose}^2 - 0.0385468 \times \text{time}^2 \quad (5)$$

When the levels of each variable are expressed in the original units, the real problem equation can accurately describe the response based on the levels of each individual factor.[69] Altering the coefficients to account for the portions of each single component, combined with placing the intercept away from the middle of the plan space, shows that this equation is not suitable for establishing the comparative condition of all the variables.[70]

A graphical representation of the association between the predicted and actual values is illustrated in Fig. 12(a) and (b). A variety of techniques were employed to remove CIP from Co/Al-LDH–CS/PVDF, such as perturbation plots, Box–Cox plots, highly studentized residuals, and residual *versus* run analysis. The reliability of the statistical model is evidenced by the strong concordance between the expected and experimental standards, as depicted in Fig. 12(c) and (d). Also, the association between the residuals and CIP adsorption procedure is demonstrated in this figure.[14] The model seems very accurate and good because there are a lot of points scattered close to zero and they are packed in that area. Any errors or patterns that the model might have missed can be seen by looking at the expected and actual numbers.[71] The Box–Cox graphs shown in Fig. 12(e) are very important in determining which transformation is the most suitable for changing the response variable. The best lambda value is found at the lowest point on the Box–Cox plot, representing the revised lambda model with the smallest sum of squares. At the lowest point of the Box–Cox plot, this perfect lambda value results in the least residual sum of squares for the updated model.[15,71] The graphs depicting the suitability of the

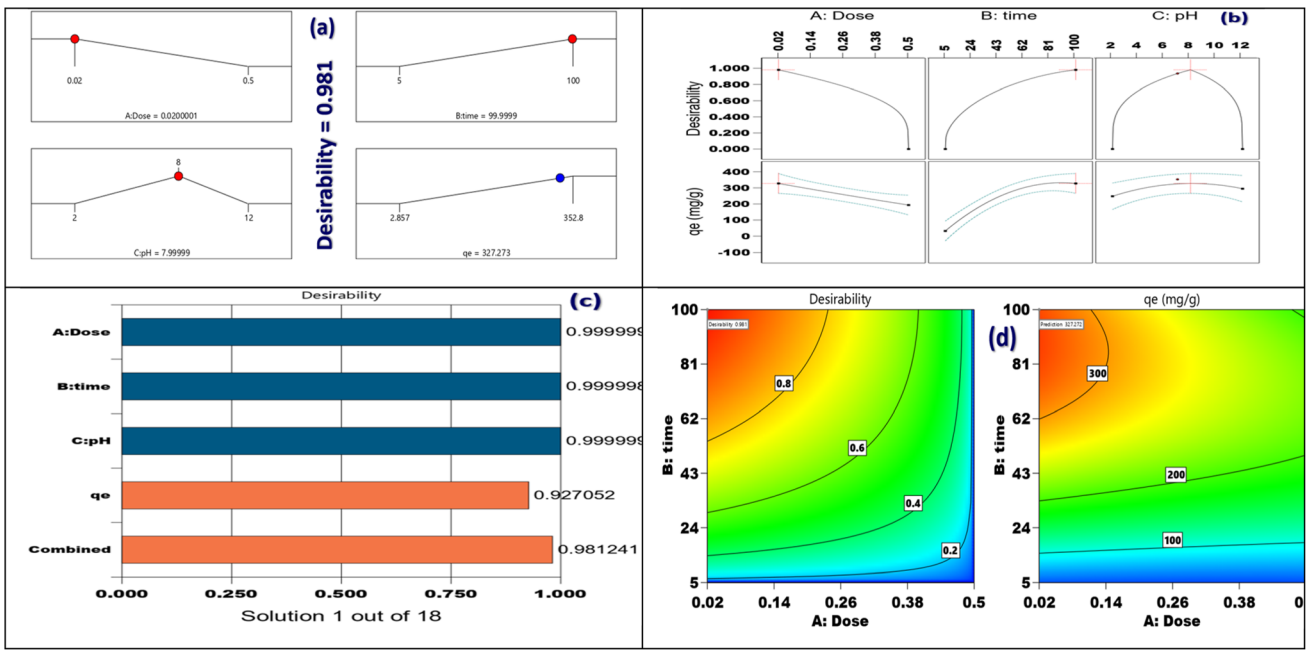

Fig. 14 (a) Increasing curiosity in finding the most statistically optimal solutions, (b) attractiveness of each response, (c) visual representation of the attractiveness of each individual in the form of a bar chart, and (d) overall attractiveness of a response.

model attest to its effectiveness. One parameter was varied while keeping all others constant to study its effect on the yield. Each parameter appears capable of enhancing the adsorption properties.[15] The time, pH, and dosage factors were determined to be the most impactful on form, as shown by the differences depicted in the figure.[72,73] The quick effect of these two factors on the adsorption capacity is illustrated by the relationship between pH and time for the adsorption process.[74,75] According to Fig. 12(f), the parameters time, dosage, and pH have all show positive effects on the adsorption capacities in the adsorption process.[76]

3.11.1. Verifying the adequacy of the model. To systematically analyze the effects of the factors studied on CIP removal, surface response three-dimensional graphs were employed to visualize the most significant interactions among the variables involved. As illustrated in Fig. 13(a), both the dosage of Co/Al-LDH–CS/PVDF membrane and pH level significantly influenced the adsorption capacity for CIP at an equilibrium time of 100 min. It can be observed in Fig. 13(b) that as pH increases from 2 to 8, the capacity for CIP adsorption also increases with the maximum value attained at a pH of 8 when keeping the adsorbent amount equal to 0.2 g per 25 mL solution volume.[14] The analysis starts by noting the positive charge of CIP with the pH_{zpc} of the Co/Al-LDH–CS/PVDF, which is found to be 4.89. According to this, it can be inferred that the ideal pH would be 8. In Fig. 13(b), various amounts and exposure times for the Co/Al-LDH–CS/PVDF membrane toward CIP are plotted against adsorption efficiency. The results show a positive relationship where a longer contact time enhances the adsorption capacity up to 0.02 g of adsorbent after 100 min of interaction. Another aspect in Fig. 13(c) looks at different time intervals and pH regarding the capability of the membrane to adsorb CIP. The results indicate that as the pH increases, especially under alkaline conditions, the adsorption capacity improves from pH 2 to 8 before starting to decrease; a longer contact time also increases the adsorption efficiency.[14,77]

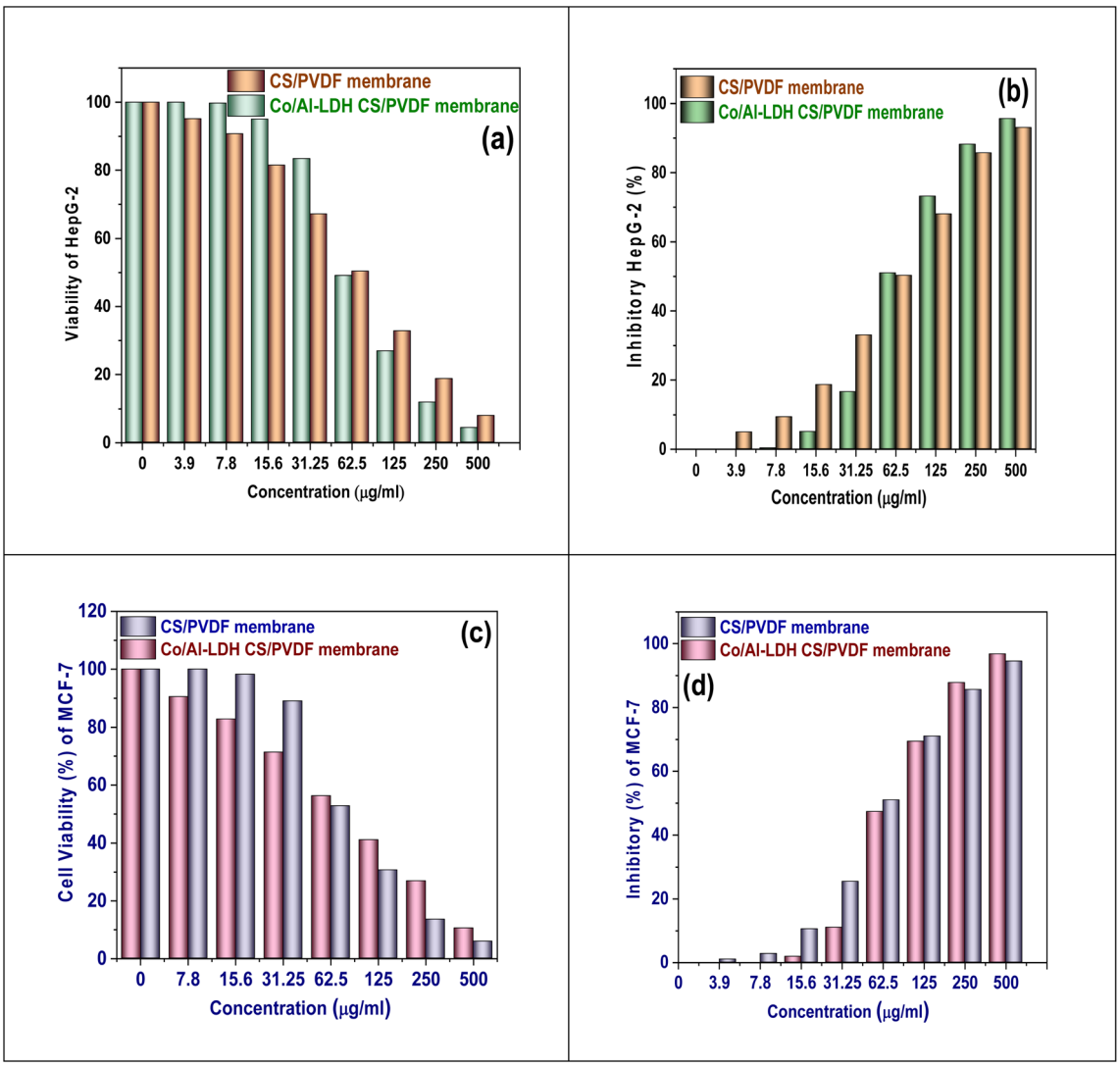

Fig. 15 Effectiveness of the CS/PVDF and Co/Al-LDH CS/PVDF nanofiber membranes regarding (a) HePG-2 cell viability, (b) HePG-2 inhibitory percentage, (c) MCF-7 cell viability, and (d) MCF-7 inhibitory percentage.

3.11.2. Model validation and the desirability method. In the analysis of the adsorption capacity for CIP (mg g^{-1}), desirability was selected to optimize the process while maintaining a compromise on the effectiveness. This strategy seeks to improve the efficiency of the process while reducing costs in terms of labor, energy, chemicals, and total operating expenses. The best results will be achieved by accurately identifying the optimal values for the factors involved.[78] The gradient of the solution proposed through mathematical optimization is beneficial, as seen in Fig. 14(a). The optimal boundaries are shown in Fig. 14(b), which are pH of 8, treatment time of 100 min, and adsorbent amount of 0.02 g. Further, desirability metrics related to each participation variable and response are expressed using a bar diagram in Fig. 14(c), giving both general and specific perspectives. In addition, Fig. 14(b) shows a typical desirability scale that starts from zero (indicating very low desirability) and goes up to one (indicating very high desirability).[77,79] This analysis assists in the validation and assessment of the accuracy of the proposed solution obtained from the mathematical optimization approach shown in Fig. 14(a). Following this, two conformity tests were conducted using the optimized variables as inputs, with the results closely matching that obtained from the numerical optimization based on an objective function. The experiment validates that BBD and RSM can accurately find the optimal adsorption conditions for the maximum yield. Additionally, Fig. 14(c) and (d) visually illustrate what we propose as the configuration for this adsorption study.[79]

3.12. Biological activity

3.12.1. Anticancer properties

3.12.1.1. HePG-2 cell line. Fig. 15(a) shows the cytotoxic effects of the PVDF/CS and Co/Al-LDH–CS/PVDF nanofiber membranes on HepG-2 cells in a dose-dependent manner, using the MTT assay after 24 hours. The results indicate a significant decrease in cell viability with increasing concentrations of both nanofiber membranes, with a greater reduction seen for Co/Al-LDH–CS/PVDF compared to PVDF/CS. At a concentration of nearly 500 μg mL^{-1}, Co/Al-LDH–CS/PVDF reduced the cell viability to below 10%, while PVDF/CS kept it at an elevated level of around 10–15%. In addition, Fig. 15(b) presents the respective inhibitory effects for each membrane, with the significant increase in inhibition clearly being concentration-dependent.[80] Co/Al-LDH–CS/PVDF showed very strong ability to inhibit, achieving close to 100% inhibition at its highest amount. PVDF/CS also had great inhibitory activity, but it was just slightly less strong. Notably, the PVDF/CS nanofiber membrane had a lower IC_{50} value of 65.89 ± 0.68 μg mL^{-1}, meaning it worked better at lower amounts. On the other hand, Co/Al-LDH–CS/PVDF had an IC_{50} of 61.62 ± 0.57 μg mL^{-1}. This means that the Co/Al-LDH–CS/PVDF membrane works better at higher amounts but that PVDF/CS is stronger at lower amounts. This shows how both materials could be very useful for treating cancer considering about dosage factors.

3.12.1.2. MCF-7 cell line. Fig. 15(c) shows the effect of PVDF/CS and Co/Al-LDH–CS/PVDF at different concentrations (0–1000 μg mL^{-1}) on the viability of MCF-7 cells over 24 h using the MTT assay. Cell viability decreased with increasing concentrations of both materials; however, this decrease was more significant for Co/Al-LDH–CS/PVDF compared to PVDF/CS. The Co/Al-LDH–CS/PVDF membrane had a strong cytotoxic effect, as demonstrated by the results. Treatment with the Co/Al-LDH–CS/PVDF membrane reduced the viability of the MCF-7 cells to less than 10% at the maximum concentration tested, while with treatment using PVDF/CS, the cell viability decreased gradually but stayed at relatively higher levels for equivalent concentrations. Furthermore, the % inhibition data in Fig. 15(d) depicts the inhibitory activity of both types of nanofiber membranes against MCF-7 cells.[81] The Co/Al-LDH–CS/PVDF membrane had a better inhibitory effect, where almost total inhibition was achieved at concentrations above 400 μg mL^{-1}. The PVDF/CS membrane only showed moderate inhibition, which came close to full suppression was not achieved. Comparing the IC_{50} values, Co/Al-LDH–CS/PVDF has much higher anticancer activity given that its IC_{50} value is 62.22 ± 1.34 μg mL^{-1}, while the PVDF/CS membrane has a higher IC_{50} of 71.6 ± 1.57 μg mL; thus, a greater concentration is required for the latter to realize 50% inhibition in MCF-7 cell proliferation. It can be concluded from these results that both nanofiber membranes have considerable anticancer activity against breast cancer cells, with the Co/Al-LDH–CS/PVDF membrane exhibiting relatively greater effectiveness.

3.12.2. Antioxidant activity. Fig. 16 shows the antioxidant activity of three different nanofiber membranes, PVDF/CS membrane, Co/Al-LDH–CS/PVDF, and ascorbic acid as a control. This evaluation was based on the DPPH free radical scavenging assay carried out under identical experimental conditions. The results demonstrate a pronounced increase in scavenging efficiency for all three samples, indicating a dose-dependent relationship over the concentration range of 0–1000 μg mL^{-1}. Ascorbic acid, marked with blue circles, was found to have the most significant antioxidant activity with

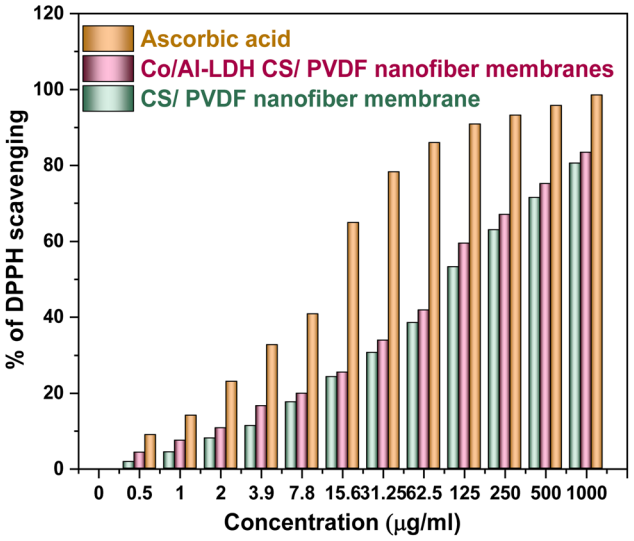

Fig. 16 Scavenging of the DPPH radical by PVDF/CS and Co/Al-LDH–CS/PVDF.

more than 90% DPPH radical scavenging at relatively low concentrations. The IC_{50} value for ascorbic acid was determined to be 11.22 ± 0.42 μg mL^{-1}, which indicates its strong free radical neutralization capability.[81] The tested nanofiber membranes showed that the PVDF/CS membrane, represented by white diamonds, had better antioxidant properties than Co/Al-LDH–CS/PVDF, which is shown by red stars. The PVDF/CS membrane achieved about 75% radical scavenging at its highest concentration tested. The IC_{50} value for this membrane was calculated to be 114.26 ± 5.08 μg mL^{-1}, indicating its moderate antioxidant activity. Co/Al-LDH–CS/PVDF had relatively low activity with an IC_{50} of 91.66 ± 3.15 μg mL; therefore, it can be concluded that both nanofiber membranes have some antioxidant activities but PVDF/CS has much more radical scavenging ability compared to Co/Al-LDH–CS/PVDF. Both membranes are less effective compared to the ascorbic acid control effect. This analysis highlights the capability of the PVDF/CS system for moderate level antioxidant applications in biomedical and environmental remediation works.

4. Conclusion

This study shows the successful creation of electrospun Co/Al-LDH mixed with CS/PVDF nanofiber membranes, which act as high-performance, multifunctional adsorbents for removing ciprofloxacin (CIP) from aqueous solutions. The combined effect of the Co/Al-LDH–CS/PVDF nanofiber framework results in a large number of accessible active sites, great structural stability, and fast adsorption kinetics. The uptake of CIP happens mainly through chemisorption influenced by different mechanisms including electrostatic interactions, hydrogen bonding, and metal–ligand coordination. The high adsorption capacity, quick time to equilibrium, and good thermodynamic characteristics of this material highlight its large potential for treating pharmaceutical wastewater as well as its use in advanced separation technologies. However, it should be noted that the adsorption effectiveness was mostly measured under batch conditions with model solutions; therefore, long-term stability, resistance to fouling, and membrane effectiveness in actual wastewater environments require further study. In addition, optimizing the composition of the LDH and polymer structure could further improve the selectivity and multifunctionality, expanding its potential applications in the environmental and biomedical fields. Although the laboratory results are promising, there are major issues that still pose challenges to the large-scale use of the Co/Al-LDH–CS/PVDF electrospun nanofiber membrane in industry. It is necessary to develop systems for scalable electrospinning that utilize environmentally safe solvents, while designing continuous-flow membrane modules for this technology to move from lab testing into real industrial application for wastewater treatment.

Author contributions

Fahad T. Alotaibi: conceptualization, data curation, investigation, resources, validation, visualization, writing-original draft, writing-review and editing. Ashraf A. El-Bindary: conceptualization, data curation, investigation, resources, validation, visualization, writing-original draft, writing-review and editing.

Conflicts of interest

There are no conflicts of interest to declare.

Data availability

The data that support the findings of this study are available from the corresponding author upon reasonable request.

Supplementary information (SI) is available. See DOI: https://doi.org/10.1039/d5ra08795c.

Acknowledgements

This work was supported and funded by the Deanship of Scientific Research at Imam Mohammad Ibn Saud Islamic University (IMSIU) (grant number IMSIU-DDRSP2601).

References

1 H. Kaur, N. Devi, S. S. Siwal, W. F. Alsanie, M. K. Thakur and V. K. Thakur, Metal–organic framework-based materials for wastewater treatment: superior adsorbent materials for the removal of hazardous pollutants, *ACS Omega*, 2023, **8**, 9004–9030.

2 G. Gopal, M. Nirmala and A. Mukherjee, A novel chitosan-coated Fe–Cu CNS loaded with CMC–Alginate composite for adsorptive removal of ciprofloxacin from water, *Surf. Interfaces*, 2023, **39**, 102981.

3 Q. M. Bui, T. Q. Vu, X. T. Vuong, V. D. Nguyen, L. T. N. Nguyen, Ha T. Le, H. T. H. Nguyen and V. P. Nguyen, Removal of fluoroquinolone antibiotics by chitosan–magnetite from aqueous: single and binary adsorption, *Processes*, 2023, **11**, 2396.

4 C. Sutherland, Exploring the state-of-the-art in metal-organic frameworks for antibiotic adsorption: a review of performance, mechanisms, and regeneration, *Environ. Toxicol. Chem.*, 2025, **44**, 880–894.

5 T. Chen, M. Ji, A. Liu and D. Ma, Fluorescent selenium covalent organic framework sensor of ofloxacin antibiotics, *Talanta*, 2023, **291**, 127884.

6 H. Alidadi, M. Dolatabadi, M. Mehrabpour and A. Dehghan, The efficacy of ciprofloxacin removal by Chitosan/Zeolite composite from aqueous solution: Response surface methodology, kinetic and isotherm studies, *Journal of Health in the Field*, 2017, **5**, 1–12.

7 E. M. Abd El-Monaem, A. S. Eltaweil, H. M. Elshishini, M. Hosny, M. M. Abou Alsoaud, N. F. Attia, G. M. El-Subruiti and A. M. Omer, Sustainable adsorptive removal of antibiotic residues by chitosan composites: An insight into current developments and future recommendations, *Arabian J. Chem.*, 2022, **15**, 103743.

8 N. Wang, W. Xiao, B. Niu, W. Duan, L. Zhou and Y. Zheng, Highly efficient adsorption of fluoroquinolone antibiotics

using chitosan derived granular hydrogel with 3D structure, *J. Mol. Liq.*, 2019, **281**, 307–314.

9 P. A. Demakov, S. Volynkin, D. G. Samsonenko, V. P. Fedin and D. N. Dybtsev, A selenophene-incorporated metal–organic framework for enhanced gas adsorption, *Molecules*, 2020, **25**, 4396.

10 A. Grover, I. Mohiuddin, A. K. Malik, J. S. Aulakh and K.-H. Kim, The potential of chitosan intercalated nickel/iron layered double hydroxide composites as extraction adsorbent for phthalates, *J. Environ. Chem. Eng.*, 2024, **12**, 113093.

11 L. Ma, X. Shi, X. Zhang and L. Li, Electrospinning of polycaprolacton/chitosan core-shell nanofibers by a stable emulsion system, *Colloids Surf., A*, 2019, **583**, 123956.

12 M. Al-Yaari, T. A. Saleh and O. Saber, Removal of mercury from polluted water by a novel composite of polymer carbon nanofiber: kinetic, isotherm, and thermodynamic studies, *RSC Adv.*, 2021, **11**, 380–389.

13 Z. Feyissa, G. D. Edossa, N. K. Gupta and D. Negera, Development of double crosslinked sodium alginate/chitosan based hydrogels for controlled release of metronidazole and its antibacterial activity, *Heliyon*, 2023, **9**, e20144.

14 R. T. Mogharbel, K. Alkhamis, R. Felaly, M. G. El-Desouky, A. A. El-Bindary, N. M. El-Metwaly and M. A. El-Bindary, Superior adsorption and removal of industrial dye from aqueous solution via magnetic silver metal-organic framework nanocomposite, *Environ. Technol.*, 2024, **45**, 2558–2574.

15 W. A. El-Fattah, A. Guesmi, N. B. Hamadi, A. Houas, M. T. Alotaibi, M. G. El-Desouky and A. Shahat, Novel composite from chitosan and a metal-organic framework for removal of tartrazine dye from aqueous solutions; adsorption isotherm, kinetic, and optimization using Box-Benkhen design, *Int. J. Biol. Macromol.*, 2024, **273**, 133015.

16 G. A. A. M. Al-Hazmi, A. A. Alayyafi, M. G. El-Desouky and A. A. El-Bindary, Guava seed activated carbon loaded calcium alginate aerogel for the adsorption of diclofenac sodium: Characterization, isotherm, kinetics, and optimization via Box-Behnken design, *Int. J. Biol. Macromol.*, 2024, **262**, 129995.

17 H. H. Alsharief, N. M. Alatawi, A. M. Al-bonayan, S. H. Alrefaee, F. A. Saad, M. G. El-Desouky and A. A. El-Bindary, Adsorption of Azorubine E122 dye via Na-mordenite with tryptophan composite: batch adsorption, Box–Behnken design optimisation and antibacterial activity, *Environ. Technol.*, 2023, 3496.

18 S. H. Alrefaee, M. Aljohani, K. Alkhamis, F. Shaaban, M. G. El-Desouky, A. A. El-Bindary and M. A. El-Bindary, Adsorption and effective removal of organophosphorus pesticides from aqueous solution via novel metal-organic framework: Adsorption isotherms, kinetics, and optimization via Box-Behnken design, *J. Mol. Liq.*, 2023, **384**, 122206.

19 S. D. Al-Qahtani, M. Alhasani, N. Alkhathami, K. A. Abu Al-Ola, K. Alkhamis, M. G. El-Desouky and A. A. El-Bindary, Effective levofloxacin adsorption and removal from aqueous solution onto tea waste biochar; synthesis, characterization, adsorption studies, and optimization by Box–Behnken design and its antibacterial activity, *Environ. Technol.*, 2023, 4928.

20 A. Almahri, M. Morad, M. M. Aljohani, N. M. Alatawi, F. A. Saad, H. M. Abumelha, M. G. El-Desouky and A. A. El-Bindary, Atrazine reclamation from an aqueous environment using a ruthenium-based metal-organic framework, *Process Saf. Environ. Prot.*, 2023, **177**, 52–68.

21 S. Ullah, A. u. Rehman, L. Gurbanova, T. Najam, A. M. Al-Mohaimeed, W. A. Al-Onazi, k. Khan, S. S. A. Shah and M. A. Nazir, Synthesis of MIL-88@ activated carbon composite as an efficient adsorbent for the removal of Rhodamine B, *Int. J. Environ. Anal. Chem.*, 2025, 1–19.

22 M. A. Nazir, T. Najam, K. Shahzad, M. A. Wattoo, T. Hussain, M. K. Tufail, S. S. A. Shah and A. ur Rehman, Heterointerface engineering of water stable ZIF-8@ ZIF-67: Adsorption of rhodamine B from water, *Surf. Interfaces*, 2022, **34**, 102324.

23 S. Riaz, R. Ali, R. Iqbal, T. Najam, A. M. Al-Mohaimeed, M. S. Elshikh, M. R. Karim, S. S. A. Shah and M. A. Nazir, Synthesis of CuFe-LDH/MIL-88 Composite for the Photocatalytic Degradation of Methyl Orange Dye, *ChemistrySelect*, 2025, **10**, e202500858.

24 M. A. Nazir, O. P. Kumar, R. Ali, M. A. Saeed, A. Ahmad, A. ur Rehman, P. Rosaiah, W. Al Zoubi and S. S. A. Shah, Fenton activated and visible light triggered trimetallic FeZnAl-LDH for remediation of Crystal violet dye, *J. Mol. Struct.*, 2025, **1335**, 142000.

25 G. H. Al-Hazmi, M. S. Refat, M. G. El-Desouky, F. K. M. Wali and A. A. El-Bindary, Effective removal of industrial dye from aqueous solution using mesoporous nickel oxide: a complete batch system evaluation, *Desalin. Water Treat.*, 2022, **273**, 246–260.

26 M. H. Shahrajabian and W. Sun, Seed Biology and Pharmacological Benefits of Fennel, Lavender, Thyme and Echinacea Species, *J. Stress Physiol. Biochem.*, 2025, **21**, 51–76.

27 M. S. Javed, M. A. Nazir, Z. Shafiq, S. Ullah, T. Najam, R. Iqbal, M. A. Ismail, T. L. Tamang and S. S. A. Shah, Advanced materials for photocatalytic removal of antibiotics from wastewater, *J. Alloys Compd.*, 2025, **1010**, 177926.

28 A. A. Alluhaybi, A. Alharbi, K. F. Alshammari and M. G. El-Desouky, Efficient Adsorption and Removal of the Herbicide 2,4-Dichlorophenylacetic Acid from Aqueous Solutions Using MIL-88(Fe)-NH2, *ACS Omega*, 2023, **8**, 40775–40784.

29 A. Almahri, K. S. Abou-Melha, H. A. Katouah, A. M. Al-bonayan, F. A. Saad, M. G. El-Desouky and A. A. El-Bindary, Adsorption and removal of the harmful pesticide 2,4-dichlorophenylacetic acid from an aqueous environment via coffee waste biochar: Synthesis, characterization, adsorption study and optimization via Box-Behnken design, *J. Mol. Struct.*, 2023, **1293**, 136238.

30 A. Mohammed and A. Abdullah, Scanning electron microscopy (SEM): A review, *Proceedings of the 2018*

International Conference on Hydraulics and Pneumatics—HERVEX, Băile Govora, Romania, 2018, pp. 7–9.

31 K. Vos, N. Vandenberghe and J. Elsen, Surface textural analysis of quartz grains by scanning electron microscopy (SEM): From sample preparation to environmental interpretation, *Earth-Sci. Rev.*, 2014, **128**, 93–104.

32 G. H. Al-Hazmi, A. M. A. Adam, M. G. El-Desouky, A. A. ElBindary, A. M. Alsuhaibani and M. S. Refat, Efficient adsorption of rhodamine b using a composite of Fe_3O_4@Zif-8: Synthesis, characterization, modeling analysis, statistical physics and mechanism of interaction, *Bull. Chem. Soc. Ethiop.*, 2023, **37**, 211–229.

33 N. M. El-Metwaly, H. A. Katouah, M. G. El-Desouky, A. A. El-Bindary and M. A. El-Bindary, Fabricating of Fe3O4@Ag-MOF nanocomposite and evaluating its adsorption activity for removal of doxorubicin, *J. Environ. Sci. Health, Part A: Toxic/Hazard. Subst. Environ. Eng.*, 2022, **57**, 1099–1115.

34 M. G. El-Desouky, A. Shahat, A. A. El-Bindary and M. A. El-Bindary, Description, kinetic and equilibrium studies of the adsorption of carbon dioxide in mesoporous iron oxide nanospheres, *Biointerface Res. Appl. Chem.*, 2022, **12**, 1022–1038.

35 M. G. El-Desouky, M. A. G. Khalil, M. A. M. El-Afify, A. A. El-Bindary and M. A. El-Bindary, Effective methods for removing different types of dyes – modelling analysisstatistical physics treatment and DFT calculations: a review, *Desalin. Water Treat.*, 2022, **280**, 89–127.

36 M. Abd El-Wahab and M. G. El-Desouky, Study the effect of antioxidants on biological activity and on homopolyropylene; mechanical and physical properties, *J. Indian Chem. Soc.*, 2022, **99**, 100764.

37 M. G. El-Desouky, A. A. El-Bindary and M. A. El-Bindary, Low-temperature adsorption study of carbon dioxide on porous magnetite nanospheres iron oxide, *Biointerface Res. Appl. Chem.*, 2022, **12**, 6252–6268.

38 M. G. El-Desouky, A. A. El-Bindary, M. A. M. El-Afify and N. Hassan, Synthesis, characterization, theoretical calculation, DNA binding, molecular docking, anticovid-19 and anticancer chelation studies of some transition metal complexes, *Inorg. Nano-Met. Chem.*, 2022, **52**, 1273–1288.

39 M. Seah, The quantitative analysis of surfaces by XPS: A review, *Surf. Interface Anal.*, 1980, **2**, 222–239.

40 D. R. Baer and M. H. Engelhard, XPS analysis of nanostructured materials and biological surfaces, *J. Electron Spectrosc. Relat. Phenom.*, 2010, **178**, 415–432.

41 M. A. El-Bindary, M. G. El-Desouky and A. A. El-Bindary, Adsorption of industrial dye from aqueous solutions onto thermally treated green adsorbent: A complete batch system evaluation, *J. Mol. Liq.*, 2022, **346**, 117082.

42 X. Zheng, C. Pan, S. Zheng and Y. Guo, Functionalized magnetic chitosan-based adsorbent for efficient tetracycline removal: Deep investigation of adsorption behaviors and mechanisms, *Sep. Purif. Technol.*, 2024, **335**, 126212.

43 M. A. Islam, M. K. Nazal, A. A. Akinpelu, M. Sajid, N. A. Alhussain, R. E. K. Billah and L. Bahsis, Novel activated carbon derived from a sustainable and low-cost palm leaves biomass waste for tetracycline removal: Adsorbent preparation, adsorption mechanisms and real application, *Diamond Relat. Mater.*, 2024, **147**, 111375.

44 A. A. El-Bindary, M. G. El-Desouky and M. A. M. El-Afify, Thermal and spectroscopic studies of some prepared metal complexes and investigation of their potential anticancer and antiviral drug activity against SARS-CoV-2 by molecular docking simulation, *Biointerface Res. Appl. Chem.*, 2022, **12**, 1053–1075.

45 A. S. Al-Wasidi, I. I. S. AlZahrani, H. I. Thawibaraka, A. M. Naglah, M. G. El-Desouky and M. A. El-Bindary, Adsorption studies of carbon dioxide and anionic dye on green adsorbent, *J. Mol. Struct.*, 2022, **1250**, 131736.

46 T. A. Altalhi, G. A. M. Mersal, M. H. H. Mahmoud, T. Kumeria, M. G. El-Desouky, A. A. El-Bindary and M. A. El-Bindary, Adsorption of doxorubicin hydrochloride onto thermally treated green adsorbent: Equilibrium, kinetic and thermodynamic studies, *J. Mol. Struct.*, 2022, **1263**, 133160.

47 A. M. Alsuhaibani, M. S. Refat, A. A. Atta, M. G. El-Desouky and A. A. El-Bindary, Efficient adsorption and removal of tetracycline antibiotics from aqueous solutions onto nickel oxide nanoparticles via organometallic chelate, *Desalin. Water Treat.*, 2022, **277**, 190–205.

48 I. Langmuir, The constitution and fundamental properties of solids and liquids. Part I. Solids, *J. Am. Chem. Soc.*, 1916, **38**, 2221–2295.

49 H. M. F. Freundlich, Over the adsorption in solution, *J. Phys. Chem.*, 1906, **57**, 385–471.

50 M. Dubinin, The equation of the characteristic curve of activated charcoal, *Proc. Acad. Sci. USSR, Phys. Chem. Sect.*, 1947, **55**, 327–329.

51 V. P. M. I. Tempkin, Kinetics of ammonia synthesis on promoted iron catalyst, *Acta Physicochim. URSS*, 1940, **12**, 327–356.

52 S. K. Lagergren, About the theory of so-called adsorption of soluble substances, *K. Sven. Vetenskapsakad. Handl.*, 1898, **24**, 1–39.

53 W. J. Weber Jr and J. C. Morris, Kinetics of adsorption on carbon from solution, *J. Sanit. Eng. Div.*, 1963, **89**, 31–59.

54 Y.-S. Ho and G. McKay, Sorption of dye from aqueous solution by peat, *Chem. Eng. J.*, 1998, **70**, 115–124.

55 M. H. Dehghani, A. Dehghan and A. Najafpoor, Removing Reactive Red 120 and 196 using chitosan/zeolite composite from aqueous solutions: Kinetics, isotherms, and process optimization, *J. Ind. Eng. Chem.*, 2017, **51**, 185–195.

56 H. N. Tran, S.-J. You, A. Hosseini-Bandegharaei and H.-P. Chao, Mistakes and inconsistencies regarding adsorption of contaminants from aqueous solutions: a critical review, *Water Res.*, 2017, **120**, 88–116.

57 E. C. Lima, A. Hosseini-Bandegharaei, J. C. Moreno-Piraján and I. Anastopoulos, A critical review of the estimation of the thermodynamic parameters on adsorption equilibria. Wrong use of equilibrium constant in the Van't Hoof equation for calculation of thermodynamic parameters of adsorption, *J. Mol. Liq.*, 2019, **273**, 425–434.

58 B. Oladipo, E. Govender-Opitz and T. V. Ojumu, Kinetics, thermodynamics, and mechanism of Cu (II) ion sorption by biogenic iron precipitate: using the lens of wastewater treatment to diagnose a typical biohydrometallurgical problem, *ACS Omega*, 2021, **6**, 27984–27993.

59 G. A. A. Al-Hazmi, A. A. El-Zahhar, M. G. El-Desouky, M. A. El-Bindary and A. A. El-Bindary, Efficiency of Fe_3O_4@ZIF-8 for the removal of Doxorubicin from aqueous solutions: equilibrium, kinetics and thermodynamic studies, *Environ. Technol.*, 2024, **45**, 731–750.

60 A. M. Alsuhaibani, M. S. Refat, A. M. A. Adam, M. G. El-Desouky and A. A. El-Bindary, Enhanced adsorption of ceftriaxone antibiotics from water by mesoporous copper oxide nanosphere, *Desalin. Water Treat.*, 2023, **281**, 234–248.

61 M. M. Majd, V. Kordzadeh-Kermani, V. Ghalandari, A. Askari and M. Sillanpää, Adsorption isotherm models: A comprehensive and systematic review (2010–2020), *Sci. Total Environ.*, 2022, **812**, 151334.

62 S. Kalam, S. A. Abu-Khamsin, M. S. Kamal and S. Patil, Surfactant adsorption isotherms: A review, *ACS Omega*, 2021, **6**, 32342–32348.

63 H. S. AlSalem, R. A. S. Alatawi, A. A. H. Bukhari, J. S. Alnawmasi, I. Zghab, M. G. El-Desouky, M. H. Almabadi, Z. H. Alnakhli and N. H. Elsayed, Adsorption and removal of Pb (II) via layer double hydroxide encapsulated with chitosan; synthesis, characterization adsorption isotherms, kinetics, thermodynamics, & optimization via Box-Behnken design, *Int. J. Biol. Macromol.*, 2024, **283**, 137517.

64 S. D. Al-Qahtani, M. Alhasani, N. Alkhathami, K. A. Abu Al-Ola, K. Alkhamis, M. G. El-Desouky and A. A. El-Bindary, Effective levofloxacin adsorption and removal from aqueous solution onto tea waste biochar; synthesis, characterization, adsorption studies, and optimization by Box–Behnken design and its antibacterial activity, *Environ. Technol.*, 2024, **45**, 4928–4950.

65 F. T. Alotaibi, M. A. Alamri, L. M. Alneghery, A. M. Alaseem, M. G. El-Desouky and A. A. El-Bindary, Doxorubicin drug delivery using an electrospun nanofiber membrane of chitosan–polycaprolactone with metal–organic framework: Box–Behnken optimization, anticancer treatment, and antimicrobial activity, *RSC Adv.*, 2025, **15**, 49243–49268.

66 A. Guesmi, N. Ben Hamadi, W. Abd El-Fattah, M. A. El-Bindary, M. G. El-Desouky and A. A. El-Bindary, Structural, thermodynamics, and mechanistic insights into a tobacco-waste derived activated carbon/polysaccharide composite sponge for efficient Cr(vi) adsorption and reusability, *RSC Adv.*, 2025, **15**, 48816–48846.

67 A. M. Alsuhaibani, A. A. Alayyafi, L. A. Albedair, M. G. El-Desouky and A. A. El-Bindary, Efficient fabrication of a composite sponge for Cr(VI) removal via citric acid cross-linking of metal-organic framework and chitosan: Adsorption isotherm, kinetic studies, and optimization using Box-Behnken design, *Mater. Today Sustain.*, 2024, **26**, 100732.

68 H. H. Alsharief, N. M. Alatawi, A. M. Al-bonayan, S. H. Alrefaee, F. A. Saad, M. G. El-Desouky and A. A. El-Bindary, Adsorption of Azorubine E122 dye via Na-mordenite with tryptophan composite: batch adsorption, Box–Behnken design optimisation and antibacterial activity, *Environ. Technol.*, 2024, **45**, 3496–3515.

69 N. B. Hamadi, A. Guesmi, W. Abd El-Fattah, M. A. El-Bindary, M. G. El-Desouky and A. A. El-Bindary, Eco-engineered electrospun La/Rb-MOF/chitosan–PCL nanofibrous membrane for high-performance, recyclable, and sustainable Cr(VI) removal from water, *RSC Adv.*, 2025, **15**, 44766–44796.

70 M. G. El-Desouky and A. A. El-Bindary, Magnetic metal-organic framework (Fe_3O_4@ZIF-8) nanocomposites for adsorption of anionic dyes from wastewater, *Inorg. Nano-Met. Chem.*, 2024, **54**, 81–95.

71 W. A. El-Fattah, A. Guesmi, N. Ben Hamadi, M. G. El-Desouky and A. Shahat, A green synthesis of cellulose nanocrystals biosorbent for remediation of wastewater containing industrial dye, *Colloids Surf., A*, 2024, **681**, 132729.

72 N. B. Hamadi, A. Guesmi, W. A. El-Fattah, M. A. El-Bindary, M. G. El-Desouky and A. A. El-Bindary, Box–Behnken optimization of stimuli-responsive DOX@Ag-MOF/chitosan — Polycaprolactone nanofiber membranes for smart controlled drug delivery and multifunctional therapeutic applications, *Int. J. Biol. Macromol.*, 2025, **330**, 147989.

73 N. A. H. Alshammari, N. H. Elsayed, A. S. Alhawiti, R. A. S. Alatawi, A. A. H. Bukhari, J. S. Alnawmasi, K. B. Alomari, K. M. Alnahdi, H. A. Al-Aoh, M. A. Al-Duais and M. G. El-Desouky, Sustainable nanofibrous cellulose-based hydrogel beads derived from cigarette filter waste, functionalized with hyaluronic acid and encapsulated in chitosan/polyethylenimine for enhanced nickel (II) adsorption from aqueous media, *Int. J. Biol. Macromol.*, 2025, **322**, 146780.

74 A. H. Jawad, U. K. Sahu, M. S. Mastuli, Z. A. ALOthman and L. D. Wilson, Multivariable optimization with desirability function for carbon porosity and methylene blue adsorption by watermelon rind activated carbon prepared by microwave assisted H3PO4, *Biomass Convers. Biorefinery*, 2024, **14**, 577–591.

75 A. H. Jawad and S. Surip, Upgrading low rank coal into mesoporous activated carbon via microwave process for methylene blue dye adsorption: Box Behnken Design and mechanism study, *Diamond Relat. Mater.*, 2022, **127**, 109199.

76 A. H. Jawad, A. S. Abdulhameed, M. M. Hanafiah, Z. A. ALOthman, M. R. Khan and S. Surip, Numerical desirability function for adsorption of methylene blue dye by sulfonated pomegranate peel biochar: modeling, kinetic, isotherm, thermodynamic, and mechanism study, *Korean J. Chem. Eng.*, 2021, **38**, 1499–1509.

77 A. Mohammed Alsuhaibani, A. A. Alayyafi, L. A. Albedair, M. G. El-Desouky and A. A. El-Bindary, Synthesis and characterization of metal–organic frameworks based on thorium for the effective removal of 2,4-dichlorophenylacetic pesticide from water: Batch adsorption and Box-Behnken Design optimization, and evaluation of reusability, *J. Mol. Liq.*, 2024, **398**, 124252.

78 N. Hassan, A. Shahat, A. El-Didamony, M. G. El-Desouky and A. A. El-Bindary, Equilibrium, Kinetic and Thermodynamic studies of adsorption of cationic dyes from aqueous solution using ZIF-8, *Moroc. J. Chem.*, 2020, **8**, 624–635.

79 H. M. Nassef, G. A. A. M. Al-Hazmi, A. A. Alayyafi, M. G. El-Desouky and A. A. El-Bindary, Synthesis and characterization of new composite sponge combining of metal-organic framework and chitosan for the elimination of Pb(II), Cu(II) and Cd(II) ions from aqueous solutions: Batch adsorption and optimization using Box-Behnken design, *J. Mol. Liq.*, 2024, **394**, 123741.

80 N. S. Moosavi and Y. Yamini, Growth of bimetallic Ni-Co MOFs on a skeleton of electrospun PAN nanofibers and coating on a thin film for SPME of amitriptyline and nortriptyline in urine and plasma samples, *J. Pharm. Biomed. Anal.*, 2023, **236**, 115755.

81 D. K. Patel, S.-Y. Won, E. Jung and S. S. Han, Recent progress in biopolymer-based electrospun nanofibers and their potential biomedical applications: A review, *Int. J. Biol. Macromol.*, 2025, 139426.